Quarterly Journal of the
Royal Meteorological Society   RMetS

Dynamics of extreme wind events in the marine and terrestrial sectors of coastal Antarctica

Thomas Caton Harrison | **John C. King** | **Thomas J. Bracegirdle** | **Hua Lu**

British Antarctic Survey, Cambridge, UK

Correspondence
Thomas Caton Harrison, British Antarctic Survey, Cambridge, CB3 0ET, UK.
Email: thoton@bas.ac.uk

Abstract

Antarctic coastal surface winds affect ice-sheet stability, sea ice, and local ecosystems. The strongest coastal winds are especially important due to the nonlinear relationship between wind speed and wind stress. We investigate the dynamics of extreme coastal winds using a simplified momentum budget calculated across the period 2010–2020 from the ERA5 reanalysis. The pressure-gradient forcing term in the budget is decomposed into a large-scale component and one associated with the temperature deficit layer. The role of budget terms across the coastal sector is compared for weak and strong winds. We then calculate composites of the top 100 easterly wind events across six east Antarctic coastal sectors, identifying terms responsible for the evolution of coastal extremes. A simple balance of terms exists offshore, dominated by large-scale forcing, contrasting with the complex balance in the onshore sector where katabatic forcing is large. Large-scale forcing explains 57% of offshore coastal wind-speed variance overall, improving to 81% when budget terms associated with the temperature deficit layer and horizontal advection are included, with significant regional variation. The residual term plays an increasingly active role as wind speed increases. Extremes in all coastal sectors are associated with a synoptic-scale transient dipole of pressure anomalies driving warm-air advection. Although katabatic forcing is a very large term in magnitude, it is found to play a passive role, declining as wind speeds increase during extreme conditions. In some regions, an anomalous southerly component develops during extremes, which we attribute to an ageostrophic barrier wind. This research underscores the major role for large-scale forcing in Antarctica's coastal winds, but also reveals a significant regional locally driven component. The results have implications for improving numerical model simulations of coastal easterlies and for studying their impacts on ocean circulation, sea ice, and ice-shelf basal melt.

KEYWORDS

Antarctica, coastal winds, cold pool, dynamics, extremes, katabatic winds, large-scale, momentum budget

1 | INTRODUCTION

Antarctic coastal winds have both global and regional importance. They are a first-order control on the strength and structure of the Antarctic Slope Current and Antarctic Coastal Current over monthly to seasonal time-scales (Armitage *et al.*, 2018; Peña-Molino *et al.*, 2016; Thompson *et al.*, 2018). Variations in these ocean currents modify transport of warm circumpolar deep water towards the continental shelf, which affects ice-shelf basal melt (Dutrieux *et al.*, 2014; Spence *et al.*, 2014), with implications for global sea levels. Coastal winds also drive sea-ice production, advection, and loss (Blanchard-Wrigglesworth *et al.*, 2021; Mathiot *et al.*, 2012; Schmidt *et al.*, 2023) and affect coastal ecosystems (e.g., Dawson *et al.*, 2023; Labrousse *et al.*, 2018; Zheng *et al.*, 2022).

On average, low-level winds in the Antarctic coastal margins have an easterly (westward) direction (Fulton *et al.*, 2017). Climatologically, the large-scale meridional pressure and temperature gradient explain the existence of easterlies at these latitudes (van den Broeke & van Lipzig, 2003). The horizontal temperature gradient is closely tied to the Southern Annular Mode (SAM: (Bracegirdle *et al.*, 2008; Yu & Zhong, 2019a)) and coastal easterlies are moderately well correlated with the SAM on interannual time-scales (Neme *et al.*, 2022). Less clear is what controls spatiotemporal variations in the structure and dynamics of the coastal easterlies and their interaction with the complex Antarctic terrain, ice sheets, and sea ice. Previous studies emphasise that Antarctic surface flow is coupled to orography, exhibiting high directional constancy and persistence (Parish, 1982; Parish & Bromwich, 1987) due to katabatic flow in the near-surface layer and blocking and baroclinicity induced by the steep slopes (Fulton *et al.*, 2017; Parish & Cassano, 2003). However, the coastal easterlies over East Antarctica have a relatively weak seasonality despite katabatic flow being much stronger during winter (van den Broeke & van Lipzig, 2003). Furthermore, easterlies extend offshore well beyond where steep slopes are capable of generating drainage flow (Fulton *et al.*, 2017), with katabatic flow typically ceasing abruptly inland of the coast (Renfrew, 2004). Both large-scale forcing and local processes appear to be important for coastal easterlies, but a detailed momentum budget analysis is needed to disentangle the two.

The role of infrequent, high-intensity events for Antarctic precipitation and temperature extremes has been the subject of numerous recent studies (e.g., Turner *et al.*, 2019; Turner *et al.*, 2021; Wei *et al.*, 2019; Wille *et al.*, 2021; Xu *et al.*, 2023). By contrast, relatively little research has examined the dynamical drivers of variability in coastal winds on daily time-scales. Near the coast, extreme winds play a disproportionate role in driving ocean currents due to the nonlinear relationship between wind speed and wind stress (Lin *et al.*, 2020; Wu *et al.*, 2016). Wang *et al.* (2021) also show how strong coastal winds can substantially enhance polynya formation and coastal sea-ice production. Strong coastal winds can also be disruptive for coastal ecosystems, including nesting birds (Descamps *et al.*, 2023). Studying their dynamics may also shed light on the role that large-scale and locally driven forces play in the coastal momentum budget on short time-scales.

Existing studies suggest the strongest coastal winds are driven by extratropical cyclones interacting with Antarctic orography (de Brito Neto *et al.*, 2022; Turner *et al.*, 2009; Weber *et al.*, 2016; Yu & Zhong, 2019b) rather than by katabatic drainage flow on its own. In addition, studies of extreme winds at polar latitudes emphasise the role of low-level jet formation due to blocking and baroclinicity (Guest *et al.*, 2018; Heinemann & Zentek, 2021; Moore & Renfrew, 2005; Petersen *et al.*, 2009; Tuononen *et al.*, 2015). The Antarctic coastal margins in turn are a productive source of cold air masses capable of generating intense baroclinicity (van de Berg *et al.*, 2008; Uotila *et al.*, 2011; Papritz *et al.*, 2015; Vignon *et al.*, 2020; Orr *et al.*, 2021), but the importance of these cold air masses (or 'cold pools') for the coastal easterlies remains poorly understood, especially offshore where the daily time-scale variability is highest (Caton Harrison *et al.*, 2022).

In this article, we aim to quantify the relative roles of large-scale and locally driven processes as drivers of Antarctic coastal wind variability and understand their evolution during the course of extremes. To achieve this, we compare actual winds in ERA5 with terms from a simplified momentum budget and analyse composited extreme wind events. We distinguish and compare two key processes driving the coastal winds based on the budget decomposition technique applied by van den Broeke and van Lipzig (2003). The first of these processes, large-scale forcing, characterises the the pressure-gradient forcing due to synoptic variability. The second, locally driven forcing, represents near-surface variations in the pressure-gradient forcing due to the temperature deficit that forms over Antarctica, as well as horizontal advection. With this framework, we address three research questions (RQ1–3).

RQ1. How does the balance of near-surface momentum-budget terms differ between onshore and offshore coastal sectors of Antarctica?

RQ2. How much Antarctic sub-daily surface wind variability in ERA5 can be explained by large-scale forcing? How does this compare for different wind-speed ranges?

RQ3. How does the momentum budget evolve during the course of Antarctic coastal wind extremes?

The reanalysis, momentum budget, and compositing approach are described in Section 2. We then address RQ1 by evaluating the magnitude of momentum-budget terms across the coastal sector in Section 3.1.1. The role of budget terms for surface wind variability is then tested in Sections 3.1.2 and 3.1.3. Finally, Section 3.2 analyses the synoptic setup and balance of momentum-budget terms through the evolution of coastal extremes. The relevance and significance of the findings is discussed in Section 4, with a summary and conclusions in Section 5.

2 | DATA AND METHODS

2.1 | ERA5

The fifth generation in the European Centre for Medium-range Weather Forecasts (ECMWF) reanalysis series, ERA5, is the most recent reanalysis product. The full technical description of the setup is given by Hersbach *et al.* (2020). Underpinning the dataset is a 2016 version of the operational ECMWF Integrated Forecasting System (IFS) model (cycle 41r2) and a hybrid incremental 4D-Var data assimilation methodology. ERA5 is available hourly on a regular 0.25° grid at 31 km horizontal grid spacing and on 137 vertical levels. 10-m winds from ERA5 are used throughout the analysis, as well as mean sea-level pressure, model-level winds, and model-level temperature for the composites in Section 3.2.

2.1.1 | Fidelity of ERA5

ERA5 is selected for this analysis as it exhibits the best overall performance against offshore and onshore observations of low-level winds in the Antarctic coastal margins compared with other current reanalyses, including near-surface temperatures (Caton Harrison *et al.*, 2022; Tetzner *et al.*, 2019; Zhu *et al.*, 2021). A previous evaluation of reanalyses (including ERA5) across Antarctica shows that all products exhibit varying bias through the seasonal cycle, which the authors suggest is related to the strength of katabatic forcing during winter (Dong *et al.*, 2020). They also highlight how complex orographic effects may not be captured well by these relatively coarse products.

Prior to the present analysis, a detailed evaluation of ERA5 Antarctic coastal winds was conducted. Stations close to each of the coastal sectors were included in the evaluation. Results are presented in Caton Harrison *et al.* (2022). Several key points from this are relevant to the current study. First, ERA5 exhibits the best overall performance against onshore and offshore low-level wind observations including near-surface temperatures. Second, ERA5 is highly correlated with Advanced Scatterometer (ASCAT) observations for ice-free periods ($r = 0.91$), with a mean bias for 2010–2017 of $-0.51\,\text{m·s}^{-1}$. Lastly, variability during stronger winds is reproduced more faithfully than that at low wind speeds, but the very strongest winds are underestimated in magnitude.

A direct comparison between ERA5 and coastal surface station wind observations during the composited extremes analysed in this article is shown in Figure S1a–f in the Supporting Information. As shown in Caton Harrison *et al.* (2022), a large envelope of uncertainty exists due to the difficulty of nearest-neighbour station colocation with ERA5. Taking this uncertainty into account, however, the evolution of the winds during extremes is generally well represented at the nearest-neighbour point. At Mawson and Casey, the ERA5 colocated winds are generally biased low, with other stations also exhibiting smaller biases, but there is evidence from the envelope of uncertainty that stronger winds are present nearby. A negative wind-speed bias has also been shown in previous evaluations (Tetzner *et al.*, 2019; Vignon *et al.*, 2019).

In this analysis, we also investigate low-level baroclinicity. An advantage of ERA5 shown in Caton Harrison *et al.* (2022) is that it does not exhibit the same low-level cold bias as other widely used reanalyses MERRA-2 and JRA-55 when compared with high-resolution sonde data. In order to maximise the resolution of near-surface processes, we use ERA5 data on model levels rather than pressure levels, which is critical for the representation of temperature inversions in the lower troposphere (Palarz *et al.*, 2020).

2.2 | Domains and compositing approach

Our analysis focuses on the Antarctic coastal margins. The chosen study period is 2010–2020, providing enough samples for all of the composited 100 extreme coastal easterly events analysed in Section 3.2 to be within the top 10th percentile of strength, balanced with the high computational cost of calculating and storing momentum budgets at every grid point on model levels. Regional subdomains are selected and named after nearby coastal stations. These subdomains are referred to as offshore boxes. As in Hazel and Stewart (2019) and Neme *et al.* (2022), we also delineate a circum-Antarctic offshore domain (shown later in Figure 4), which is used in Section 3.1 to analyse budget terms more broadly. This circum-Antarctic offshore domain is drawn over offshore regions (identified using the ERA5 land–sea mask) where the mean zonal
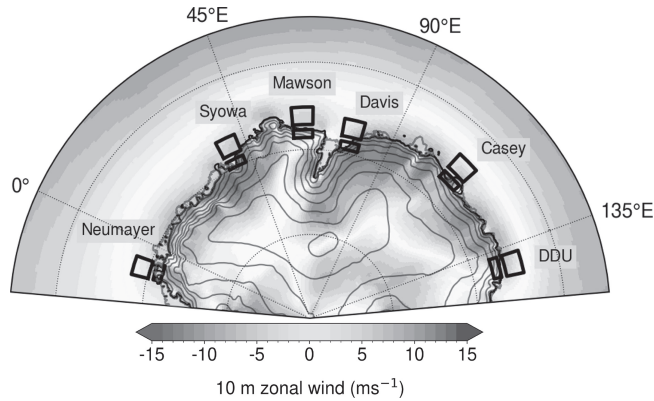
FIGURE 1 Map of domains used in this study, overlaid on mean ERA5 10-m zonal wind (m·s⁻¹, shaded) from 1979–2020. Black boxes indicate the regional domains used, including both an onshore and offshore sector. Dark grey contours show the orography at 500-m intervals (obtained from the ERA5 orography field). Light grey lines show the edges of ice shelves, obtained from the SCAR Antarctic Digital Database (Gerrish *et al.*, 2023). [Colour figure can be viewed at wileyonlinelibrary.com]

wind for the period 2010–2020 is negative to indicate prevailing easterlies. Each offshore box also has a corresponding onshore box, used to compare onshore and offshore momentum-budget evolution.

Composites are used in this article to compare similar wind events. The algorithm for selecting events for the extremes analysis in Section 3.2 is as follows.

1. Define six 'offshore box' regions, shown in Figure 1.
2. Calculate the mean six-hourly 10-m zonal wind over these regions for the period 2010–2020.
3. Order the zonal wind values from most negative (strongest easterly) to most positive.
4. For each value, check if it is in the lowest 10th percentile of zonal winds (i.e., top 10th percentile of easterly strength) for the box region and not within 4 days of a date already included in the list of composite events.
5. If both conditions are met, add the date of the value to the list of composite events until 100 events are obtained.

A four-day window is included as a condition in the algorithm above to avoid double counting of the same extreme wind event. 10-m zonal winds are used for compositing, as the prevailing flow direction is easterly. An additional advantage of using zonal winds rather than 10-m wind speed is that it ensures the individual composited events are more similar (all associated with a particular flow direction) and hence the composites themselves are more physically meaningful. This avoids, for example, cancellation of strongly easterly and strongly westerly winds in the composite. Nonetheless,

all results were also recalculated using the top 100 10-m wind speeds. No significant differences were found, with between 70 and 92 of the chosen events (out of 100) at each station overlapping between the two compositing methods.

2.3 | Momentum budget

A momentum budget is calculated to distinguish the role of large-scale and locally driven forcing. Our implementation of a momentum budget for the Antarctic coastal region follows the form described by van den Broeke *et al.* (2002), used to characterise the relative role and seasonality of budget terms Antarctica-wide in van den Broeke and van Lipzig (2003). The budget equations are a form of the Ball model (Ball, 1960), which divides the Antarctic atmosphere into a free atmosphere component and shallow well-mixed near-surface inversion layer. A review of early applications of this approach is given in Parish and Cassano (2001). The pressure gradient force divides into a large-scale component and one associated with a temperature deficit layer (TDL), defined by the difference between the actual potential temperature profile θ and a 'background' potential temperature profile θ_0. The TDL is typically defined as a near-surface layer which is diabatically cooled relative to some predefined ambient atmosphere (Parish & Cassano, 2001) and may be equivalent with the inversion layer. Here, it takes on a broader definition as a low-level atmospheric layer which is colder than expected based on a linear extrapolation of mid-tropospheric temperatures. We assume that this TDL is due to surface-related processes such as diabatic cooling due to emission of longwave radiation and hence terms relating to it are sources of 'locally driven' acceleration. In the budget as set out by van den Broeke *et al.* (2002), the effects of variations in the depth of the TDL are also accounted for, which becomes especially important close to the coast where hydraulic jump formation and sea-breeze dynamics can cause the TDL to deepen substantially (Pettré *et al.*, 1993), in turn affecting the katabatic flow near the coast (Yu *et al.*, 2005). Furthermore, the budget accounts for horizontal advection, which is usually small.

Over land, terms are calculated on a downslope/cross-slope coordinate system; a positive acceleration here means positive in the downslope direction (*y*-direction terms) or positive to the right of downslope (*x*-direction terms). Offshore, the coordinate system reverts to north–south, east–west, meaning positive is southerly (*y*-direction) and westerly (*x*-direction). Acceleration terms for the tendency of the cross-slope wind (u) and down-slope wind (v) are obtained from components of the

momentum budget based on the form in van den Broeke *et al.* (2002):

$$\frac{\partial u}{\partial t} = \underbrace{-u\frac{\partial u}{\partial x} - v\frac{\partial u}{\partial y}}_{\substack{\text{Horizontal Advection} \\ (\text{advh}_u)}} + \underbrace{\frac{g}{\theta_0}\frac{\partial \hat{\theta}}{\partial x}}_{\substack{\text{Shallow Baroclinicity} \\ (\text{sbc}_x)}}$$

$$\underbrace{+fv}_{\substack{\text{Coriolis Forcing} \\ (\text{cor}_x)}} \underbrace{-fv_{\text{lsc}}}_{\substack{\text{Large-Scale Forcing} \\ (\text{lsc}_x)}} - R_u, \quad (1)$$

$$\frac{\partial v}{\partial t} = \underbrace{-u\frac{\partial v}{\partial x} - v\frac{\partial v}{\partial y}}_{\substack{\text{Horizontal Advection} \\ (\text{advh}_v)}} + \underbrace{\frac{g}{\theta_0}\frac{\partial \hat{\theta}}{\partial y}}_{\substack{\text{Shallow Baroclinicity} \\ (\text{sbc}_y)}} \underbrace{-fu}_{\substack{\text{Coriolis Forcing} \\ (\text{cor}_y)}}$$

$$\underbrace{+fu_{\text{lsc}}}_{\substack{\text{Large-Scale Forcing} \\ (\text{lsc}_y)}} + \underbrace{\frac{g}{\theta_0}\Delta_\theta \sin\alpha}_{\substack{\text{Katabatic Forcing} \\ (\text{kat})}} - R_v, \quad (2)$$

where x and y are the cross-slope and downslope direction (reverting to zonal and meridional offshore), g is gravitational acceleration, α is the surface slope angle, Δ_θ is the difference between θ and θ_0 (see below), $\hat{\theta}$ is Δ_θ integrated between the top of the previously defined top of the TDL and the surface, u_{lsc} and v_{lsc} are the large-scale cross-slope and downslope wind, respectively, and f is the Coriolis parameter. The terms R_u and R_v in the momentum budget absorb any other sources of acceleration in the cross-slope and downslope directions respectively, and are obtained by calculating the residual between the sum of the estimated terms and the actual u or v time derivative in ERA5. These include the effects of friction and turbulence as well as the vertical advection term. All horizontal gradients are estimated on ERA5's hybrid height coordinates (i.e., terrain-following), except in the calculation of the large-scale forcing term. Individual components of this momentum budget are referred to throughout the article with the notation in brackets below each term.

The key underlying uncertainty in the momentum-budget approach is how the potential temperature (θ) is distinguished from the background potential temperature (θ_0). θ_0 should be as close as possible to the actual θ, with the exception of the lowest layer of the Antarctic atmosphere, which tends to be diabatically cooled. Sometimes the TDL is quite shallow and capped by an inversion layer, but it may also extend several thousand metres above ground level. In Parish and Cassano (2001), estimation of θ_0 is achieved by a linear fit to θ between 1500 and 5000 m above ground level (a.g.l.), which is then extrapolated to the surface (on sigma levels). In van den Broeke *et al.* (2002), θ_0 is again obtained by extrapolation, though, based on fig. 5 therein, the chosen heights within which

the linear fit is calculated may have been higher, as a temperature deficit layer extends up above 4000 m a.g.l.

In our approach, θ_0 is obtained by selecting a model level m in ERA5 (level 100, corresponding to approximately 4300 m a.g.l.), calculating the mean value of θ at that level m, interpolating the data to levels of constant θ, then extrapolating based on a linear fit to the vertical θ gradient between the selected theta level and the one 20 K lower (i.e., lower in the atmosphere). Values of θ_0 found to be lower than θ as a result of this are reverted to θ. The result of this was a smooth interpolated field of θ_0 down to the surface across Antarctica and in different seasons, including at sub-daily time-scales. The rationale for selecting an m of 100 is detailed further in Appendix A.

To obtain the large-scale forcing, we first assume that the large-scale wind (u_{lsc}, v_{lsc}) well above the TDL is equal to the geostrophic wind (u_g, v_g), which is estimated on pressure levels with

$$u_g = -\frac{g}{f}\frac{\partial z}{\partial y} \quad (3)$$

and

$$v_g = \frac{g}{f}\frac{\partial z}{\partial x}, \quad (4)$$

where z refers to the geopotential height. The level at which $u_{\text{lsc}} = u_g$ is set at 300 hPa. To obtain u_{lsc} and v_{lsc} on higher pressure levels (i.e., nearer the surface), they are scaled by assuming thermal wind balance with the horizontal gradient of θ_0 following

$$\frac{\partial u_{\text{lsc}}}{\partial \ln p} = \frac{R_d}{f}\left(\frac{p}{p_0}\right)^{R_d/c_p}\frac{\partial \theta_0}{\partial y} \quad (5)$$

and

$$\frac{\partial v_{\text{lsc}}}{\partial \ln p} = -\frac{R_d}{f}\left(\frac{p}{p_0}\right)^{R_d/c_p}\frac{\partial \theta_0}{\partial x}, \quad (6)$$

where p is pressure (with p_0 a reference pressure, here 1000 hPa) and R_d and c_p are the gas constant and specific heat capacity for dry air, respectively. The resulting values of u_{lsc} and v_{lsc} are subsequently interpolated onto ERA5's hybrid height levels.

A key term in Equation (2) is the katabatic forcing or *kat*. This term captures the buoyancy-driven flow, which is large over the steep coastal slopes where slope angle (α) is large. *kat* also depends on background temperatures and a sharply defined TDL.

Another key term is the shallow baroclinicity or *sbc*. *sbc* only tends to become large in the coastal margins (van den Broeke & van Lipzig, 2003), but as a representation of the thermal wind induced by changes in the depth of the temperature deficit layer it quantifies the effect of baroclinicity

at low levels due to long-wave cooling, as well as other diabatic processes. In the coastal margins, these could include cold-air pooling due to orographic effects, advection, or sea breezes. Our interpretation of the term is that in a coastal context it represents the effects of low-level baroclinicity not captured by large-scale gradients in θ_0. As the large-scale term also includes a thermal wind, we refer to this term as the shallow baroclinicity, rather than the thermal wind term as used elsewhere in the literature.

To understand the role of budget terms in explaining variance in the surface winds, we compare the actual ERA5 wind speed with the balanced winds derived by assuming steady-state flow with acceleration terms balanced by the Coriolis force, that is, the time derivative goes to zero in Equations (1) and (2):

$$-fv = -u\frac{\partial u}{\partial x} - v\frac{\partial u}{\partial y} + \frac{g}{\theta_0}\frac{\partial \hat{\theta}}{\partial x} - fv_{\text{lsc}} - R_u, \quad (7)$$

$$fu = -u\frac{\partial v}{\partial x} - v\frac{\partial v}{\partial y} + \frac{g}{\theta_0}\frac{\partial \hat{\theta}}{\partial y} + fu_{\text{lsc}} + \frac{g}{\theta_0}\Delta_\theta \sin\alpha - R_v. \quad (8)$$

By dividing both sides of Equation (7) by $-f$ and Equation (8) by f to obtain them in terms of v and u, respectively, then neglecting non-large-scale terms, our balanced flow estimate of the vector magnitude of the large-scale wind becomes

$$|\boldsymbol{lsc}| = \sqrt{v_{\text{lsc}}^2 + u_{\text{lsc}}^2}. \quad (9)$$

To understand the role of non-large-scale terms, we compare this with the balanced flow obtained by including other active terms in the budget (i.e., all except the residual), which we refer to as $|\boldsymbol{A}|$:

$$|\boldsymbol{A}| = \sqrt{\left(\frac{-u\frac{\partial v}{\partial x} - v\frac{\partial v}{\partial y} + \frac{g}{\theta_0}\frac{\partial \hat{\theta}}{\partial y} + fu_{\text{lsc}} + \frac{g}{\theta_0}\Delta_\theta \sin\alpha}{f}\right)^2 + \left(\frac{-u\frac{\partial u}{\partial x} - v\frac{\partial u}{\partial y} + \frac{g}{\theta_0}\frac{\partial \hat{\theta}}{\partial x} - fv_{\text{lsc}}}{-f}\right)^2}. \quad (10)$$

3 | RESULTS

3.1 | Wider role of budget terms

3.1.1 | Long-term mean balance of budget terms

Coriolis forcing is large at high latitudes and winds adjust relatively rapidly to geostrophic equilibrium. As a result, x-direction winds (cross-slope onshore, zonal offshore) are generally well correlated with the y-direction pressure-gradient forcing (downslope onshore, meridional

offshore) terms from Equation (2) and vice versa, giving the balanced flow in Equation (8) when the acceleration is relatively small. Zonal flows, including the coastal easterlies, respond at large scales to pressure gradients in the meridional direction. These y-direction terms (Figure 2) are larger than the x-direction terms (Figure 3). When describing y-direction terms, we are describing terms most relevant to the zonal winds (e.g., easterlies), and vice versa for x-direction terms.

The relative size and sign of budget terms differs greatly between the onshore and offshore sector. In most offshore sectors, a simple balance exists between large-scale forcing (the largest active term), Coriolis forcing, and the residual term (Figure 2) for y-direction terms. lsc_y is consistently positive offshore, indicating easterlies (in geostrophic balance). At Mawson and Dumont D'Urville (DDU) (Figure 2c,f), shallow baroclinicity is also large offshore. Onshore, the picture is more complex, with the largest terms being katabatic forcing and large-scale forcing, balanced by Coriolis forcing, shallow baroclinicity, and the residual. Very near the coast, a complex interplay of terms, occurs with horizontal advection becoming large as well. Katabatic forcing peaks 200–250 km inland at Neumayer, Syowa, Davis, and Casey (Figure 2a,b,d,e), but at Mawson and DDU it peaks very close to the coast (Figure 2c,f).

The x-direction terms are generally smaller (accounting for variations in meridional winds in geostrophic balance). Large-scale forcing remains the largest active term offshore, but its sign differs regionally (Figure 3a–f). At Mawson (Figure 3c), a positive lsc_x indicates large-scale southerly flow, whereas at Syowa (Figure 3b) negative lsc_x indicates large-scale northerly flow. Section 3.2.4 addresses how the meridional flow component can differ so substantially between two relatively nearby stations by considering the evolution of the flow during extremes.

Judging by the magnitude of the terms, large-scale forcing is not dramatically larger than others in the coastal sectors sampled. However, changes in the flow through time occur due to momentum-budget imbalances; such imbalances may be driven by terms that are not the largest in magnitude (Chen et al., 2020). To understand the contribution of budget terms to short time-scale variability, we next correlate their vector magnitude with the evolution of surface wind speed at each grid point in ERA5.

3.1.2 | Role of budget terms in short-time-scale variability

Across Antarctica and the Southern Ocean, surface wind speed is weakly to moderately well correlated with the $|\boldsymbol{lsc}|$ term from Equation (9) alone (Figure 4a). Within the domain of the offshore coastal easterlies indicated by
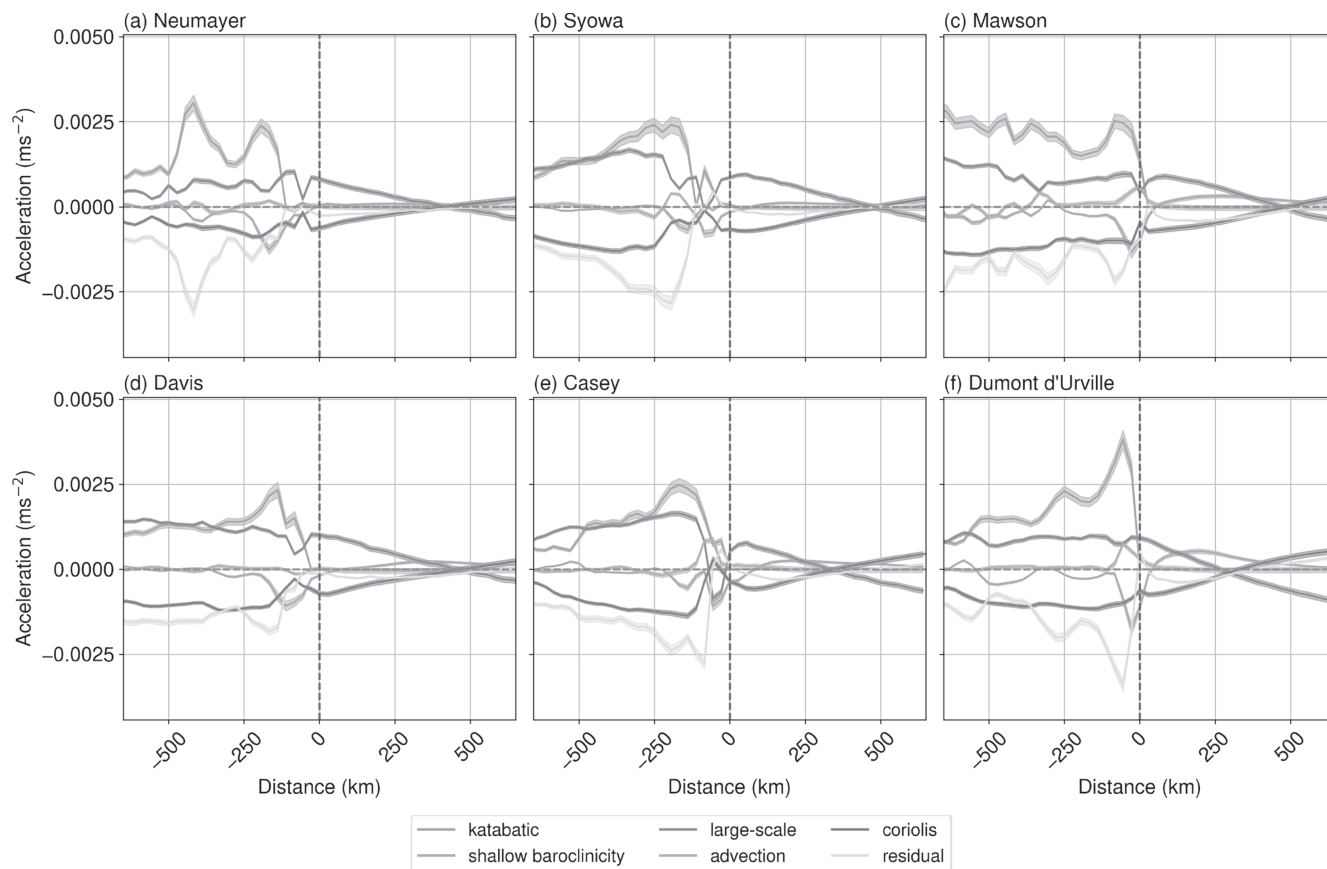
FIGURE 2 Cross-sections of 10-m y-direction momentum-budget terms at the centroid longitude of each offshore box, averaged over the period 2010–2020. The horizontal axis is distance from the location of the coastal stations for each region, with negative values of distance indicating higher latitude (further onshore) and positive values lower latitude (further offshore). Shaded envelopes indicate the 95% confidence interval. A vertical dashed red line indicates the latitude of the station. Panels include (a) Neumayer, (b) Syowa, (c) Mawson, (d) Davis, (e) Casey, and (f) DDU. [Colour figure can be viewed at wileyonlinelibrary.com]

the dashed black line, a spatial mean r^2 of 0.57 indicates that |$\textbf{\textit{lsc}}$| explains 57% of the surface wind-speed variance. Regions where r^2 is relatively low include those over complex orography (such as the Transantarctic Mountains near 170°E and south of 70°S), over the Ross and Filchner–Ronne Ice Shelves, and over steeply sloping sectors of coastal Antarctica. Over the plateau, r^2 is relatively high, demonstrating the connection between surface winds and large-scale processes in the Antarctic interior, as shown for the South Pole on decadal time-scales by Neff (1999). Some offshore sectors exhibit comparatively low r^2, including off Adélie land (140°E), the Mawson coast and Cape Darnley (65°E), and east of the Antarctic Peninsula (60°W). Large-scale forcing is noticeably better at explaining offshore coastal winds in the West Antarctic sector (60°W to 180°) compared with much of East Antarctica, where large regions of weaker correlation are found.

When katabatic forcing (*kat*), shallow baroclinicity (*sbc*), and horizontal advection (*advh*) are added to obtain the term |$\textbf{\textit{A}}$| (Equation 10), r^2 increases in many regions and decreases in a small number of regions (Figure 4b).

Within the offshore coastal easterly domain, the spatial mean r^2 increases to 0.81. The largest impact of these terms is over ice shelves where pooling of cold air generates shallow baroclinicity, over confluence regions and steeply sloping terrain where katabatic drainage flow is strong, and over the offshore coastal margins.

The residual terms R_u and R_v are needed to explain the remaining wind-speed variance (Figure 4c). These represent friction and other processes not captured by the momentum budget, such as gravity-wave drag and vertical advection of momentum. Such processes may induce highly ageostrophic motion, for which the simple thermal wind-balance assumption used to derive momentum-budget terms in Equations (1) and (2) are not appropriate.

Other areas with reduced r^2 seen in Figure 4b close to complex orography and near the pole are likely affected by the finite-difference approximations used to estimate gradients such as $d\hat{\theta}/dy$. In the real ECMWF IFS cycle from which ERA5 was generated, a semi-Lagrangian scheme and a spectral transform technique are used for
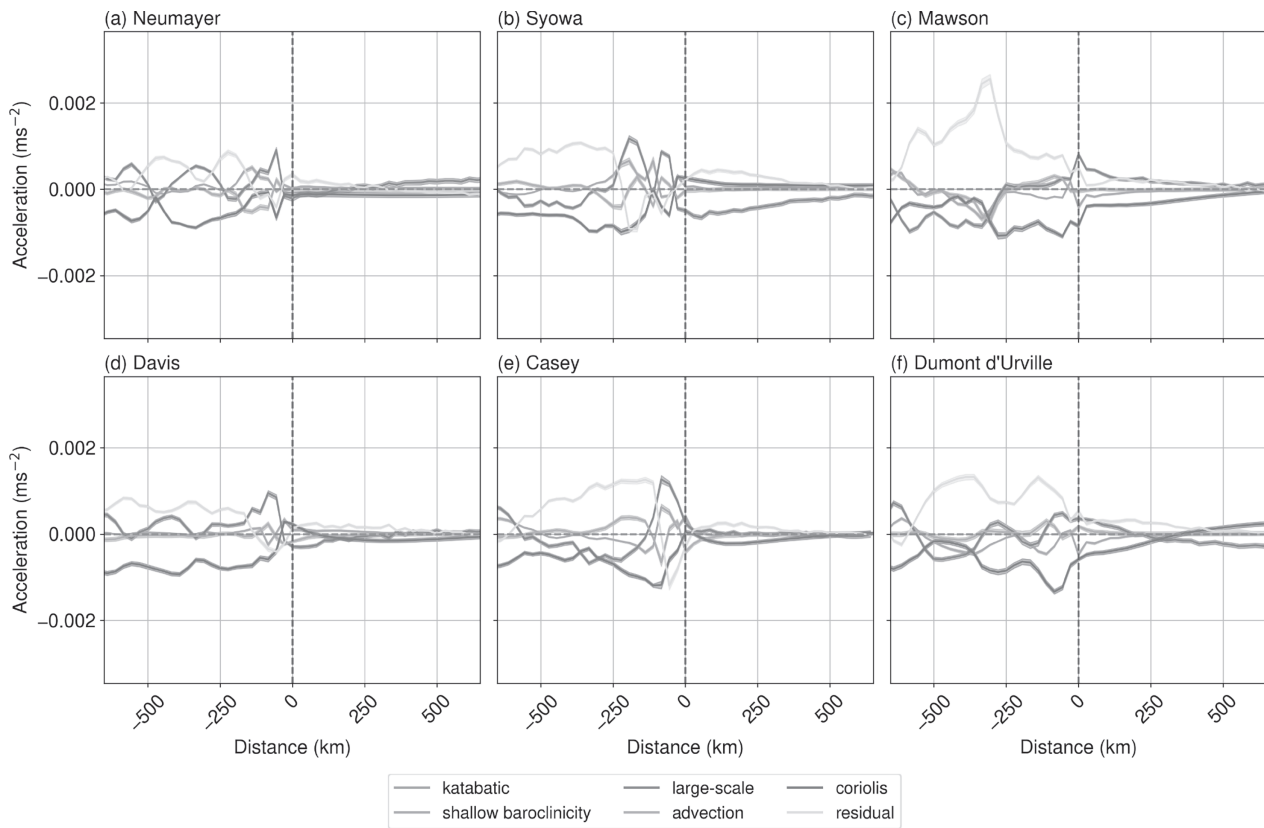
FIGURE 3 As in Figure 2 but for the *x*-direction. [Colour figure can be viewed at wileyonlinelibrary.com]
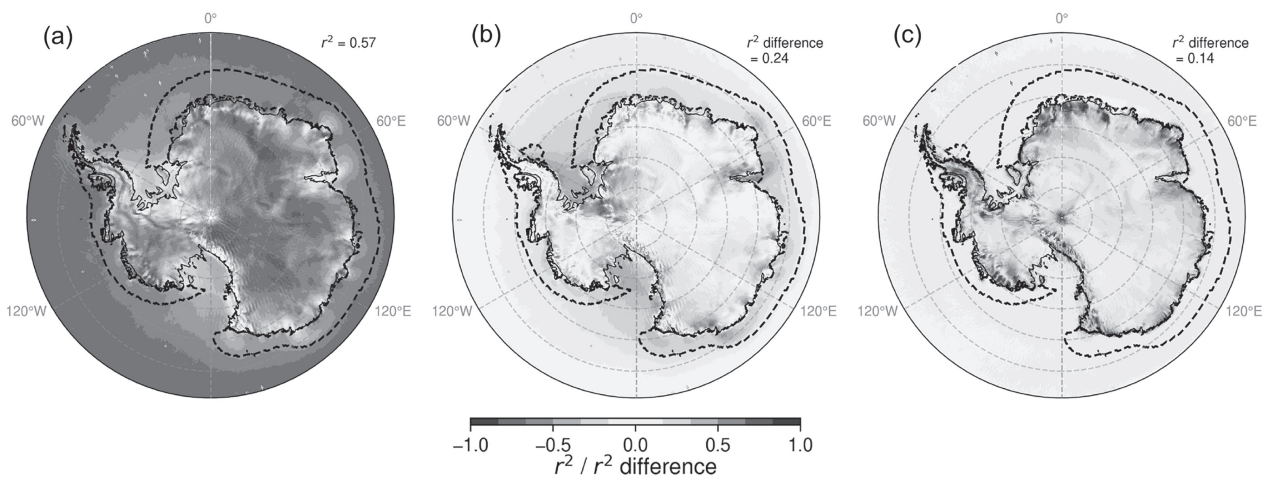

FIGURE 4 (a) Coefficient of determination for 2010–2020 (r^2) between ERA5 10-m wind speed and $|\boldsymbol{lsc}|$, (b) the additional r^2 at each grid point obtained by adding other active terms to obtain $|\boldsymbol{A}|$ (the sum of active terms, defined in Equation 10), and (c) the additional r^2 at each grid point obtained by adding the vector magnitude of the residual term R to $|\boldsymbol{A}|$. Black dashed regions indicate the coastal easterly domain, over which the r^2 values quoted in each panel and in the text are averaged. [Colour figure can be viewed at wileyonlinelibrary.com]

discretisation of momentum-budget equations in time and space. The calculation of budget terms in spectral space could result in a smoother wind field over regions with sharp discontinuities, such as near complex topography or the coast.

In summary, large-scale forcing is the largest budget term offshore in magnitude and is generally the largest

contributor to explained wind variance across most of Antarctica. Other budget terms help explain additional sources of variance, especially over ice shelves and complex orography. It is possible that non-large-scale terms play a greater role in explaining changes to the wind field over longer time-scales (for example seasonal). Another possibility is that the role of the temperature deficit layer

in the momentum budget differs across wind regimes. To test this, we next examine how well $|lsc|$ and $|A|$ correlate with wind speed across three wind-speed bins.

3.1.3 | Role of budget terms across wind-speed ranges

Although large-scale forcing is the leading-order budget term, its relationship to wind speed and the role of other terms varies with wind speed. During weak to moderate wind states (0–10 m·s^{-1}, Figure 5a), large-scale forcing as estimated in Equation (9) is more effective as a predictor of wind-speed variance over the plateau than in terrestrial coastal sectors. In the coastal margins (delineated with the dashed black line) and over the Southern Ocean, $|lsc|$ is only moderately correlated with surface wind speeds. Inclusion of other budget terms (Figure 5b) is critical for these weaker winds, especially over the coastal slopes, confluence region, and offshore coastal margins. The residual term still has an active role in many regions (Figure 5c), especially the coastal slopes, where a complex balance of terms exists (Figure 2) and gravity-wave drag is likely to be important.

During strong winds (10–20 m·s^{-1}, Figure 5d), $|lsc|$ alone is a better predictor of surface wind speed over most of the coastal slopes than when combined with other terms such as $|A|$ (Figure 5e), except over certain confluence regions (e.g., south of the Amery Ice Shelf at 70°E). Additional terms in $|A|$ still play an important role offshore, especially around east Antarctica. This is due predominantly to the *sbc* term (not shown) and suggests that pooling of cold air, local diabatic cooling, and sea-breeze circulations are important. At these wind speeds, the residual term is critical (Figure 5f) to explaining surface winds onshore and contributes significantly offshore as well as suggesting that complex terrain-driven flows play a role over the marine sector of coastal Antarctica.

Interestingly, the peak extreme winds over 20 m·s^{-1} (Figure 5g–i) are almost entirely restricted to the Antarctic onshore and offshore coastal sectors, with other regions masked due to a lack of samples. At these highest wind speeds, the samples are dominated by short-lived instances of rapidly evolving flow, which are likely separated by long periods of weaker winds. Furthermore, the size of the tendency term itself may become non-negligible, with winds approximating less well to a balanced flow. $|lsc|$ alone is weakly correlated with the wind speed during these peak winds (Figure 5g), improved in some regions such as the offshore Mawson coast (60–70°E) when other active terms are added (Figure 5h). The residual term is very important (Figure 5i), accounting for errors in estimation of the budget terms and unresolved processes, which

may have a large impact during these highly transient states.

The very strongest extreme winds as shown in Figure 5g–i are likely to occur at a local scale over a period of hours and may not be represented reliably in a coarse reanalysis, as suggested when comparing a single grid point with real observations in Figure S1. When we describe extreme winds in the next section, our focus is not on the very short-lived dynamics occurring at the peak (time-scale of hours), but rather on the evolution through the course of the entire event (time-scale of days). In addition, we average over the regions shown in Figure 1 and over 100 events to reduce noise, such that peak composite-mean offshore winds typically fall within the 15–20 m·s^{-1} range.

3.2 | Extreme coastal wind events

3.2.1 | Synoptic conditions

The top 100 extreme coastal wind events within all offshore boxes are associated with a low mean sea-level pressure (MSLP) anomaly situated offshore, with a high-pressure anomaly located to the east (Figure 6). The composite MSLP anomaly patterns for each offshore box are strikingly similar. Each region's offshore box at lag 0 ($T + 0H$) is situated at the southern flank of a low-pressure anomaly, which is apparently deformed by the coastal terrain, with high-pressure anomalies also extending to the south over the continent, maximising the pressure gradient. Over the high interior of the continent, MSLP may not be a meaningful variable, as it is derived by extrapolating surface pressure to sea level over a deep layer. However, composite anomaly patterns for 600 hPa height (not shown), which lies above the surface over much of Antarctica, are very similar to those for MSLP. Lagged composites from $T - 72H$ to $T + 72H$ (Figures S2–S7, panels a–g respectively) indicate that the decay of the system is relatively rapid following the peak, such that the dipole of anomalies is significantly weaker at $T + 48H$ than $T - 48H$ (comparing panels b and f).

A large negative zonal wind anomaly occurs in all sectors by definition (Figure 7, middle row). Interestingly, the meridional wind anomaly differs greatly by sector. This is discussed further in Section 3.2.4. Warm-air advection aloft induces a positive temperature anomaly, which is particularly pronounced during the $T - 24H$ to $T + 24H$ period shown in Figure 7, and in all cases a sloping sector of lower or slightly negative temperature anomalies is found offshore in the lowest 1000 m and extending 200–400 km offshore (Figure 7 top row). We refer to this latter feature as the coastal 'cold pool'. The post-peak
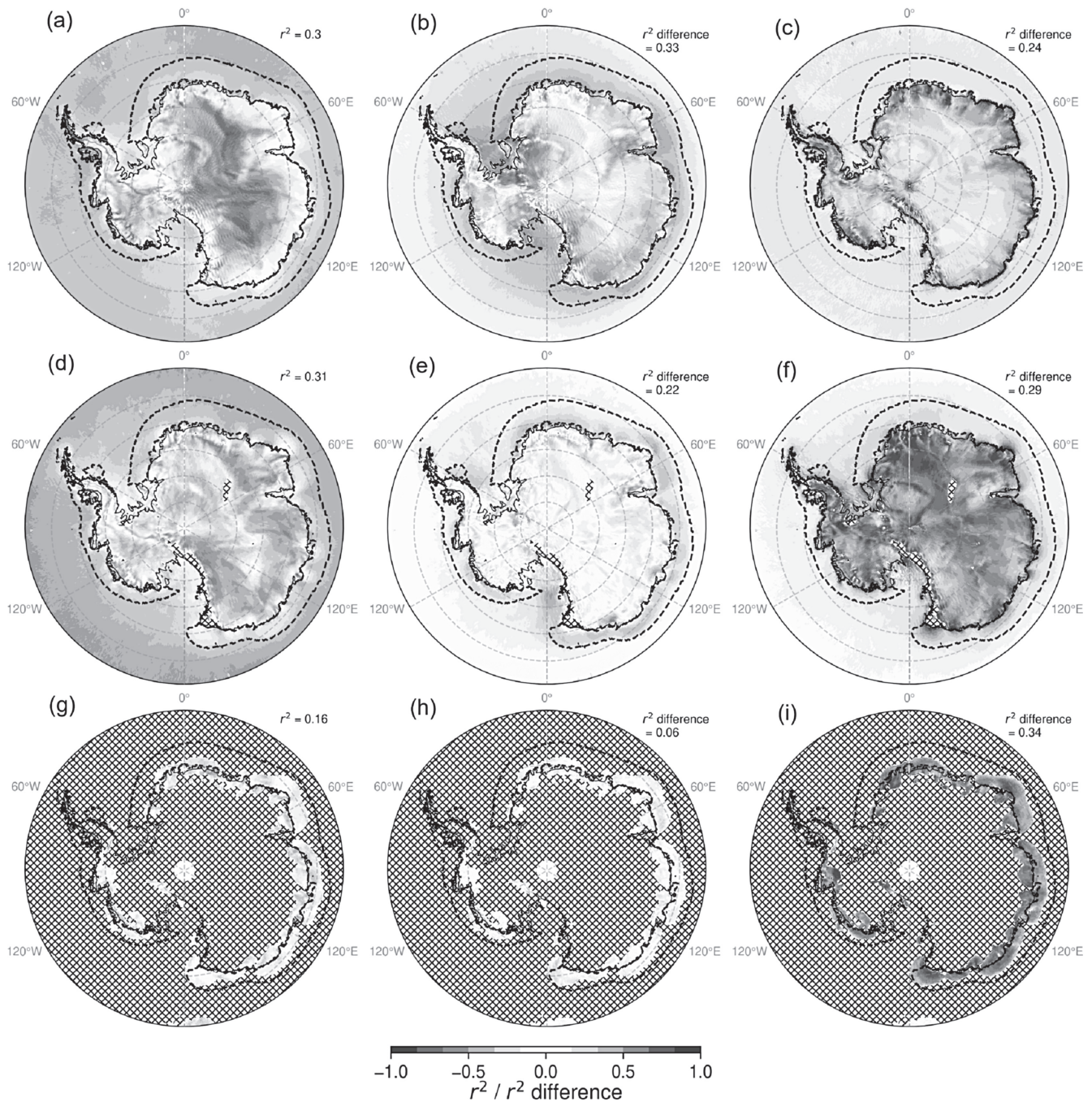
FIGURE 5 As in Figure 4 but for the subset of wind speeds in the ranges (a–c) 0–10, (d–f) 10–20, and (g–i) 20–30 m·s^{-1}. Grid points with fewer than 100 available data point in the corresponding wind-speed category are masked with hatching. [Colour figure can be viewed at wileyonlinelibrary.com]

and pre-peak temperature profiles differ substantially; whereas $T - 66H$ to $T - 24H$ are generally associated with a weakly negative temperature anomaly in the lower troposphere with regionally varying levels of offshore extension (Figure S8a–f, top row), $T + 24H$ to $T + 66H$ consistently exhibit low-level horizontally homogeneous warm anomalies (Figure S9a–f, top row).

The coastal cold-pool feature varies in its structure and intensity around the East Antarctic coastal margins.

At Neumayer, the cold pool is more diffuse and decoupled from a warm anomaly over the Ekström Ice Shelf in the lowest 100 m (Figure 7a, at the location of the vertical dashed grey line). By contrast, at Mawson, Casey, and DDU, the cold pool is quite well defined (Figure 7c–e respectively). At these stations there is also a near-zero or slight cold anomaly extending inland within a layer approximately 200–400 m above ground level, with warm anomalies below. The structure of these anomalies is quite
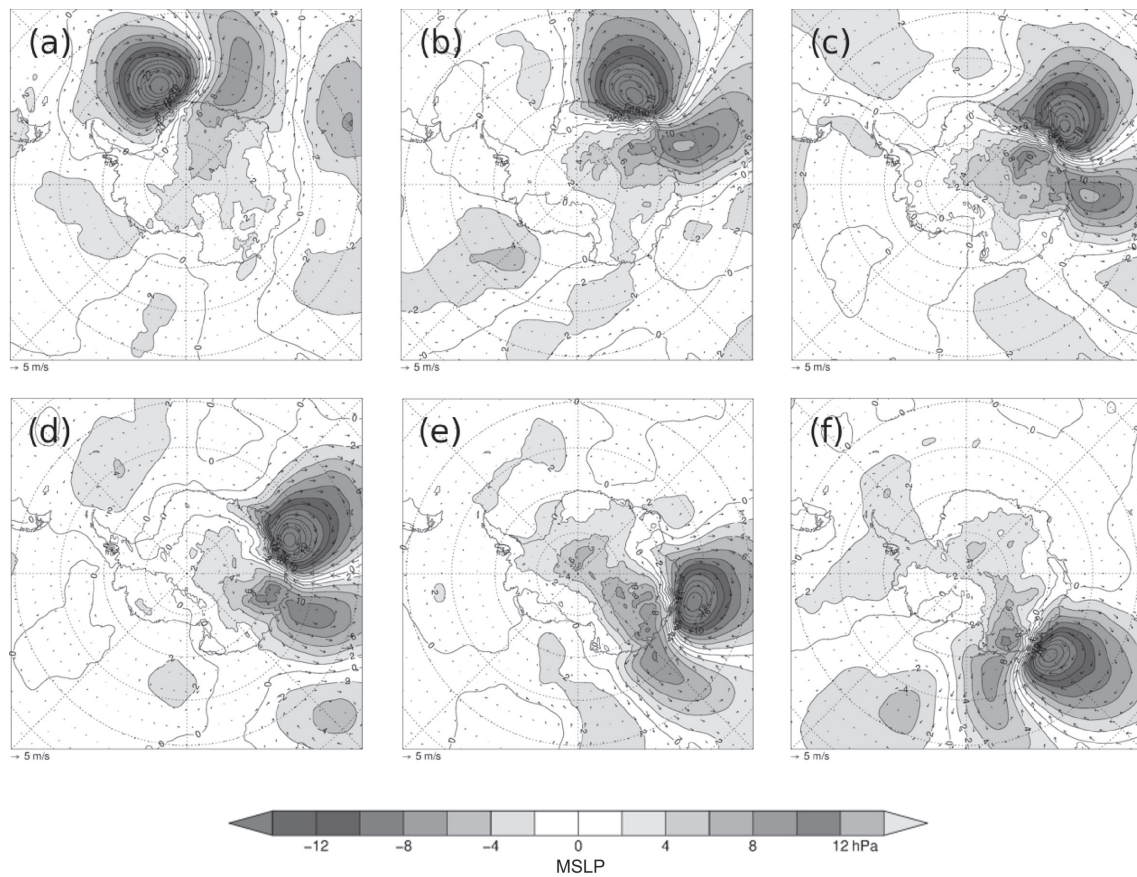
FIGURE 6 Composite mean ERA5 MSLP (shaded) and 10-m wind (arrows) anomalies with respect to 2010–2020 averaged across the 100 extreme coastal wind events for each region indicated, including (a) Neumayer, (b) Syowa, (c) Mawson, (d) Davis, (e) Casey, and (f) DDU. [Colour figure can be viewed at wileyonlinelibrary.com]
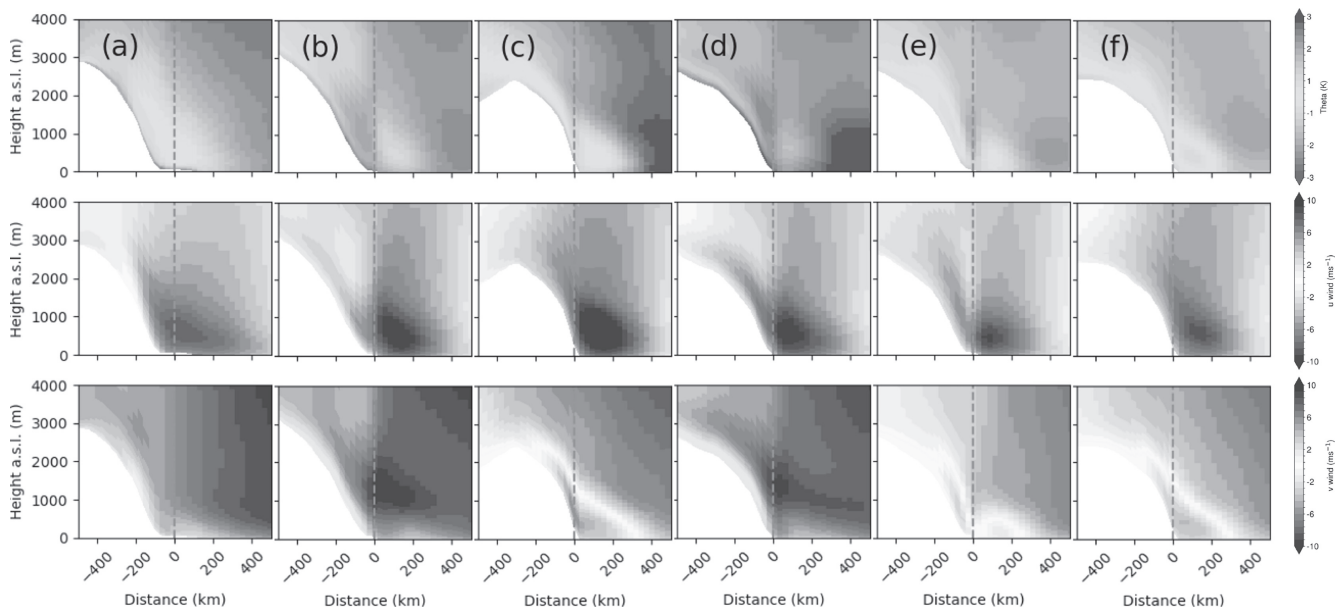

FIGURE 7 Composite cross-sections of anomalies with respect to 2010–2020 of Theta (K, upper), zonal wind (m·s^{-1}, middle), and meridional wind (m·s^{-1}, bottom) from ERA5 averaged across the lag period $T - 24H$ to $T + 24H$ at the centroid longitude of each offshore box. Columns are (a) Neumayer, (b) Syowa, (c) Mawson, (d) Davis, (e) Casey, and (f) DDU. The horizontal axis is distance from the location of the coastal stations for each region, with negative values of distance indicating higher latitude (further onshore) and positive values lower latitude (further offshore). [Colour figure can be viewed at wileyonlinelibrary.com]
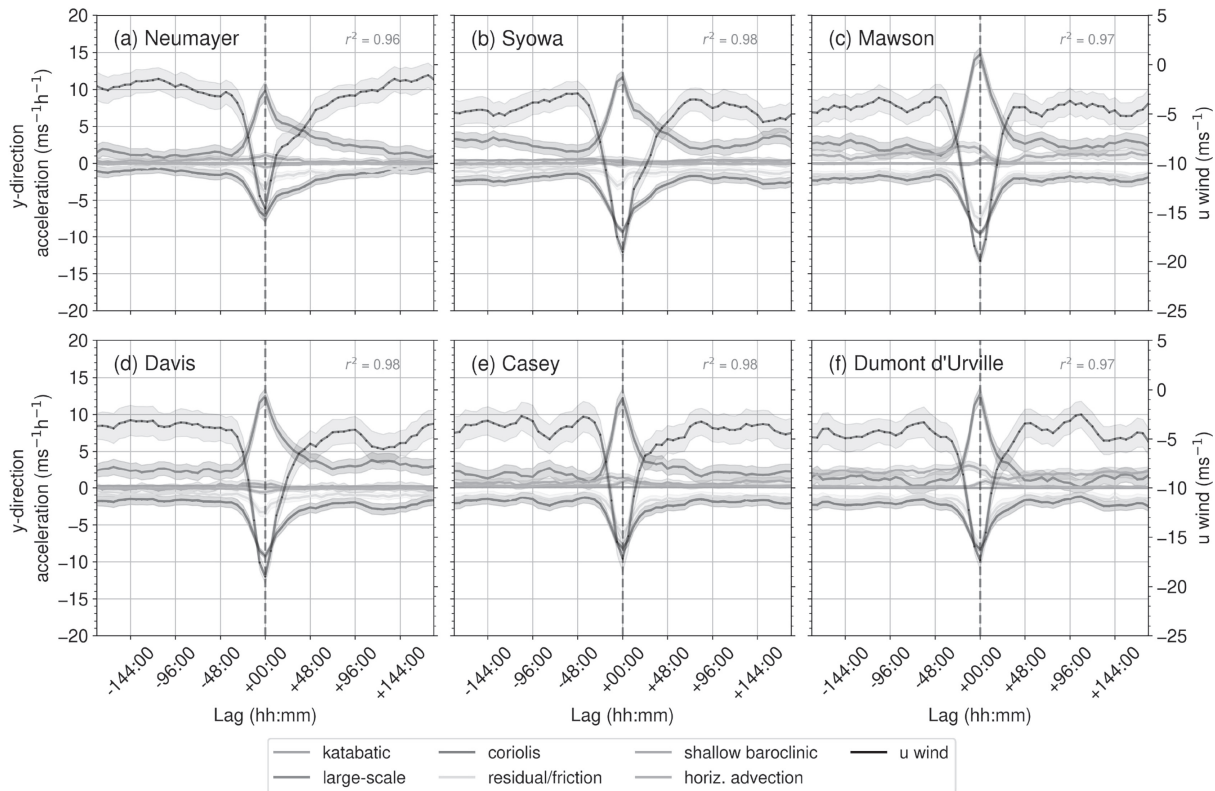
FIGURE 8 Composite time series of mean 10-m y-direction momentum-budget terms averaged across each of the regional offshore boxes, with shaded envelopes indicating the 95% confidence interval. The vertical dashed grey line indicates lag 0. Panels include (a) Neumayer, (b) Syowa, (c) Mawson, (d) Davis, (e) Casey, and (f) DDU. The solid black line and grey envelope indicate the 10-m zonal wind and its 95% confidence interval respectively, plotted on the right-hand vertical axis. r^2 values quoted indicate the coefficient of determination between the u wind and the y-direction large-scale forcing term (lsc_y). [Colour figure can be viewed at wileyonlinelibrary.com]

similar to the pattern shown by Vignon *et al.* (2020) in simulations of a strong coastal wind event at DDU, in which they identify cold-air pileup over the coastal sea ice, followed by katabatic jump formation and 'backfolding' of low-level isentropes and trapped gravity-wave formation, inducing vertical motion and drag on the flow near the surface. Evidence of a decoupled cold anomaly over land at Mawson, Casey, and DDU persists during the post-peak period (Figure S7c–e).

3.2.2 | Offshore momentum-budget evolution

In the coastal margins of Antarctica, the dominant flow direction is zonal. As a result, here we focus primarily on the acceleration terms in the y-direction (downslope–upslope onshore and north–south offshore), which, in geostrophic balance, account for x-direction winds.

In the lead-up to peak winds, each station is subject to an increase from mean 10-m u winds (i.e., at $T - 48H$) of between 0 and $-5\,\text{m·s}^{-1}$ up to a peak of -15 to $-20\,\text{m·s}^{-1}$

(at $T + 0H$: Figure 8). In this pre-peak state, the large-scale forcing and shallow baroclinicity are balanced by the Coriolis force and friction (residual), with a negligible contribution from horizontal advection.

As the composite time series approaches the peak ($T + 0H$), each region in Figure 8 broadly follows the same pattern: the large-scale acceleration term begins to increase substantially 24–36 h prior to $T + 0H$ before reaching a peak and then declining gradually over the following 48 h. At all stations, the mean surface 10-m u winds are highly correlated with the lsc_y term (between 96% and 98% of the variance explained), indicating a major role for large-scale forcing through the course of the event. The v winds are not as consistently well correlated with the lsc_x term. For instance, at Mawson, Casey, and DDU, the r^2 between the 10-m v wind and lsc_x is 0.0, 0.11, and 0.11 (Figure S10c,e,f) compared with 0.83, 0.91, and 0.88 at Neumayer, Syowa, and Davis (Figure S10a,b,d), with other regional disparities onshore (Figure S11a–f). It should be noted that the high correlation with lsc_y is not necessarily inconsistent with the much greater role for the residual term suggested by Figure 5. Correlations calculated for Figure 8 track the evolution of individual events, whereas correlations in

Figure 5 for the strong–extreme categories are only for the period when the winds are at their strongest and are calculated across many separate events at individual grid points.

The magnitude of the Coriolis acceleration term is quite consistent across the sampled regions, which is unsurprising, as all are found at similar latitudes and have similar peak wind speeds. A larger point of difference is the magnitude of the residual term. At Syowa and Davis (Figure 8b,d), the large-scale term is principally balanced by the Coriolis term, whereas at Casey and DDU (Figure 8e,f) the residual term nearly equals the Coriolis term in magnitude. Regional differences in these residual terms could be due to variations in nearby terrain, orography, and sea-ice cover, which can introduce frictional effects, as well as unresolved processes such as gravity-wave drag. A larger friction term at Mawson is also expected relative to Neumayer, for example, because of the greater u wind magnitude shown in Figure 8c relative to Figure 8a.

On average, the shallow baroclinic term sbc is secondary in magnitude to large-scale forcing offshore during the strongest wind events. The only sampled regions where the term becomes large are Mawson and Dumont d'Urville (Figure 8c,f). The term retains a near-constant magnitude from $T - 48H$ to $T + 0H$, however, and does not increase in response to the arrival of the low-pressure disturbance. This constancy suggests that the shallow baroclinicity responsible for the high sbc is set up by the background conditions rather than the anomaly. Nevertheless, the extreme wind conditions have a clear impact on sbc following the peak (from around $T + 12H$ onwards), with an approximately 50% decline in the term's magnitude at DDU (Figure 8f) and a decline to near zero at Mawson (Figure 8c).

Horizontal advection plays a near-negligible role in the evolution of each of the regions' composite momentum budgets.

3.2.3 | Onshore momentum-budget evolution

Onshore, momentum budget composites follow a similar pattern to the offshore sector but are combined with the additional influence of the katabatic acceleration term (Figure 9). In the pre-peak state (at $T - 48H$), the katabatic forcing and large-scale forcing are balanced by the shallow baroclinic term, Coriolis force, and friction, again with a near-zero contribution from horizontal advection.

Similarly to the offshore sector, between 95% and 98% of the composite time-series variance in the 10-m u wind is explained by lsc_y (Figure 9a–f). The peak in large-scale forcing onshore lags behind the offshore peak, occurring

approximately 6 h later. This is likely due to the trajectory of the cyclone (e.g., Figure S2), which moves southward from $T - 24H$ to $T + 0H$, reaching the offshore box (from which the composited dates are identified) prior to the onshore box. Unlike the offshore sector, there are some regional differences in the magnitude of the large-scale term at the event peak. For instance at Casey (Figure 9e), the peak in large-scale forcing is muted in magnitude (near zero) compared with at DDU (Figure 9f, 5 m·s^{-1} ·h^{-1}). In all cases, the magnitude of the peak onshore is smaller than that offshore. A reduction in large-scale forcing at Casey may be due to the impact of the Law Dome, which acts as a barrier to large-scale flow.

Katabatic forcing is a major acceleration term for each of the onshore boxes sampled (Figure 9), in all cases being the largest budget term during the pre-peak period ($T - 60H$ to $T + 0H$). As shown in Section 3.1.3, however, above 10 m·s^{-1} the $|A|$ term is not as well correlated with the actual surface winds as the $|lsc|$ term over most of the onshore coastal sector. In fact, an increase in wind speeds at the event peak is not associated with an increase in katabatic forcing. Instead, the peak cross-slope winds onshore are driven primarily by an increase in large-scale forcing, with katabatic forcing actually declining in magnitude in response to the cyclone passage. This slight decline is a feature that occurs in all sampled regions, implying this is a common dynamical response to large-scale synoptic forcing. A decline in the magnitude of katabatic forcing is mirrored by a decline in the magnitude of sbc. Whereas offshore sbc is positive in the same direction as the increasing large-scale acceleration term, onshore the sbc actually opposes the flow in the direction of both the large-scale and katabatic acceleration terms. This is expected, as onshore sbc represents the deepening of the temperature deficit layer at the coast responsible for the apparently abrupt cut-soff in downslope flow found in observations and model simulations (van den Broeke & van Lipzig, 2003).

3.2.4 | Anomalous meridional winds at Mawson

As shown in Figure 7 (bottom row), an anomalous southerly develops offshore at Mawson, Casey, and DDU during the peak extreme winds. Furthermore, unlike at Neumayer, Syowa, and Davis, the v winds at these locations are poorly correlated with the lsc_x term, suggesting that the development of the southerly cannot be explained as a geostrophically balanced response to an increasing large-scale zonal pressure gradient. The southerly anomaly also has a distinct structure, which mirrors the cold anomaly (Figure 7c, top row).
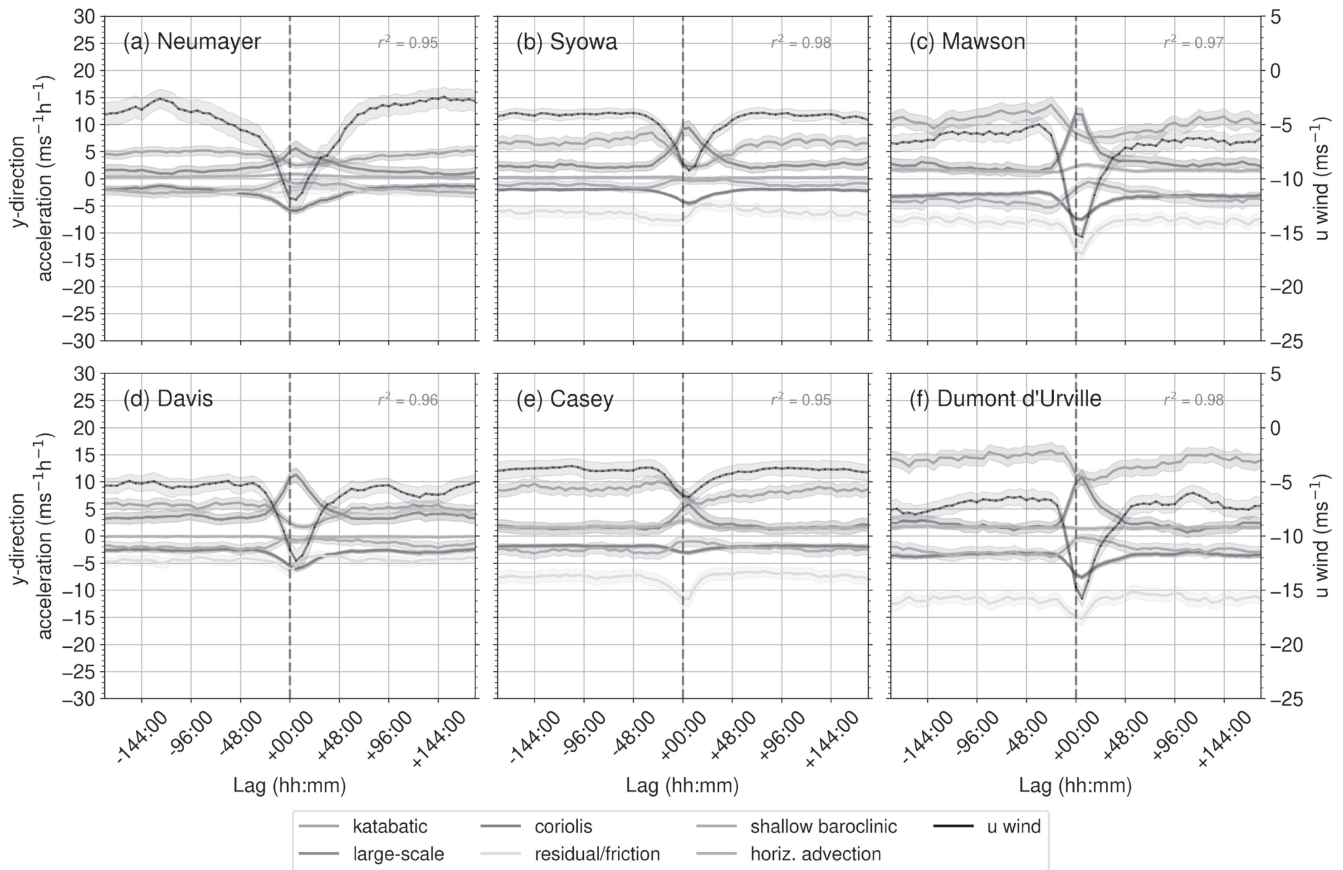
FIGURE 9 As in Figure 8 but for the onshore domain. [Colour figure can be viewed at wileyonlinelibrary.com]

To investigate the development of these winds, we compare the offshore meridional wind with the momentum-budget terms at both Mawson and Syowa. These are relatively nearby sectors of the East Antarctic coast, but during peak winds a southerly develops at Mawson, whereas a moderate northerly develops at Syowa (Figure 7b, bottom row). To test which momentum-budget terms can explain this, we correlate various x-direction terms with the meridional winds averaged over the Mawson and Syowa offshore boxes in Figure 10.

As indicated in Figure 10b, winds at Syowa are correlated very well with lsc_x alone and the development of the northerly mirrors the large northerly large-scale flow that occurs. Addition of other terms to the budget has only a small impact on the correlation, with the inclusion of the residual term scaling the magnitude of the total acceleration via friction. By contrast, the meridional wind at Mawson is entirely uncorrelated with lsc_x (Figure 10a), and the addition of other active terms has a negligible impact on the correlation. Whereas the large-scale forcing in the 24 h prior to the peak of the storm favours a northerly like at Syowa, instead winds develop a southerly component. After the peak, the large-scale term changes sign but only favours a southerly flow during the day following the peak winds. The actual meridional winds can only be explained with the inclusion of the residual term.

The apparently active role played by the residual term at Mawson suggests that an ageostrophic flow is set up where the large-scale northerly flow comes into contact with the coastal slopes. On short time-scales, an ageostrophic flow directly away from the coast is typical of barrier-jet formation (e.g., Chen *et al.*, 2021; Overland & Bond, 1995; Petersen *et al.*, 2009). Additional sources of cold air, for example due to the Amery Ice Shelf near Mawson, may support a more 'hybrid' form of barrier jet (Loescher *et al.*, 2006; Olson *et al.*, 2007), whereby continental cold-air outbreaks allow a cold pool to form off the Mawson coast, as suggested by Figure 7c (top row). A detailed analysis of barrier-jet formation is beyond the scope of this article, but the mechanism appears to be common based on the large role for the residual term around the East Antarctic coast above $10\,\mathrm{m\cdot s^{-1}}$ in Figure 5.

4 | DISCUSSION

Climatological easterlies in ERA5 extend out over ocean approximately 380 km from the shore (based on the mean distance between the northern and southern edges of
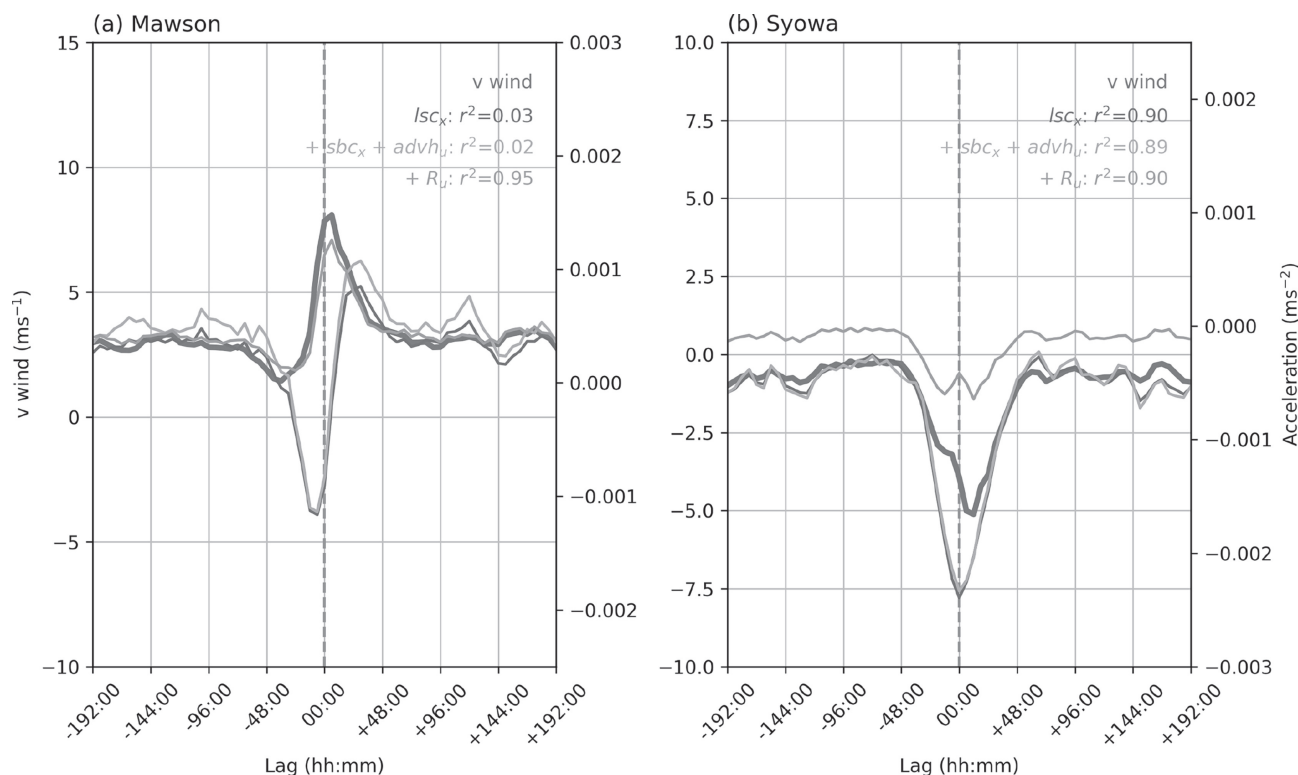
FIGURE 10 Composite time series of mean 10-m x-direction combined momentum-budget terms averaged across the offshore boxes of (a) Mawson and (b) Syowa. Variables shown include the v wind (thick dark blue), the lsc_x term (red), the sum of lsc_x, sbc_x, and $advh_u$ (pink), and the previous with R_u added (cyan). [Colour figure can be viewed at wileyonlinelibrary.com]

the red contour in Figure 1) and are found in a region uniquely prone to extreme winds. At these spatial scales, our momentum budget indicates that large-scale forcing accounts for the largest proportion of total explained variance in surface wind speed. Reanalyses such as ERA5 are limited in their capacity to capture the full range of wind speeds associated with locally driven processes. Furthermore, compared with observations, ERA5 generally underestimates the strength of the strongest winds, indicating certain processes are misrepresented, under-represented, or too local in scale to be captured by reanalysis. Nevertheless, studies of extreme winds based on in situ observations and remote sensing have also generally found that large-scale synoptic pressure patterns are crucial in the coastal sector (Ebner *et al.*, 2014; Parish *et al.*, 1993; Parish & Bromwich, 1998; Turner *et al.*, 2009; Wang *et al.*, 2021). What role, then, does locally driven forcing play in the dynamics of Antarctica's coastal winds?

In Figure 4, we show how the full variance in six-hourly wind speed cannot be explained without additional momentum-budget terms, corresponding to katabatic and shallow baroclinic forcing (as well as horizontal advection). Of these, the dominant contribution offshore within the coastal easterlies comes from pooling of cold air generating shallow baroclinicity (*sbc*). This is also a process that

plays opposite roles over the terrestrial and marine sectors of coastal Antarctica. Whereas on land it opposes katabatic flow (Gallée & Schayes, 1992) by generating isolated pockets of warm air at the foot of the coastal slopes (e.g., King *et al.*, 1998), offshore it enhances the flow by driving a thermal wind in the same direction as the background easterlies. However, we also show in Figure 5 that this contribution is greatest for weaker winds, and the residual term is critical at the highest wind speeds.

Despite the apparent importance of shallow baroclinicity for background wind variance offshore, the prominent cold-pool feature shown in Figure 7c,f at Mawson and DDU, and the size of the shallow baroclinic terms in Figure 2, the role of *sbc* in the evolution of the momentum budget during extremes is small. Key to this puzzle could be the time-scale over which the cold pool is established. Like the preconditioning of coastal isentropes by katabatic drainage flow described by Fulton *et al.* (2017), cold pooling may be set up over longer, seasonal time-scales and hence holds importance for the structure of the background flow, which is then modified primarily by large-scale forcing on shorter time-scales, especially during extremes. This could also explain why non-large-scale terms appear to play a larger role at higher wind speeds offshore in Figure 5 than suggested by the composite means; they may not change much through the

course of an individual extreme event, but they may help explain the baseline flow.

Sources of shallow baroclinicity are not well understood. One analysis of regional Antarctic heat budgets finds that horizontal advection is important in the formation of an offshore temperature deficit during austral winter (van de Berg *et al.*, 2007). We find that Mawson and DDU have both the highest katabatic acceleration terms onshore (Figure 9c,f) and shallow baroclinic terms offshore (Figure 8c,f), so it is plausible that cold airmasses advected from onshore are a key source of shallow baroclinicity. Some regions are also likely more prone to a buildup of cold air than others, due to damming effects along steep topography (Parish, 1983).

There has been discussion in the literature about whether variability and trends in the coastal easterlies are related to changes in katabatic winds. For instance, Hazel and Stewart (2019) define a pole-to-coast index to estimate the contribution of katabatic winds to changes in easterly ocean wind stress. Others have suggested that changes in pressure gradients induced by synoptic forcing can enhance katabatic winds on short time-scales (Turner *et al.*, 2009; Yu & Zhong, 2019b), given the correspondence between large synoptic pressure gradients and the most intense terrain-following winds (Parish & Bromwich, 1998). A recent analysis by Davrinche *et al.* (2023) uses the same momentum-budget approach to estimate the role of surface-driven processes (including katabatic forcing) for winds at different time-scales across an Adélie Land transect (the longitude of Dumont d'Urville). They find that, although these processes are important for seasonal and spatial variability, large-scale forcing is the most important at short time-scales, which we corroborate in this analysis.

In our momentum budget time-series analysis, we find that katabatic forcing in the coastal sector is somewhat weakened during extreme winds. This could be due to a range of factors, including warm-air advection, adiabatic descent, and turbulent mixing. We classify only the acceleration due to the temperature deficit over sloping terrain as katabatic. Under strong wind conditions, this temperature deficit is often reduced and hence the conditions are less favourable for the formation of katabatic winds. As Fulton *et al.* (2017) suggest, katabatic drainage flow may be important for setting up Antarctica's terrain-following isentropes, but based on our findings it is large-scale forcing that controls the bulk of sub-daily variability superimposed on this steady state. Bintanja *et al.* (2014) estimate the katabatic acceleration term over Antarctica in the EC-Earth global climate model and find only minor changes between the present day and end of the 21st century under the A1B SRES scenario (rapid economic growth with a balance of energy sources)

relative to changes in the large-scale term, implying this dynamical relationship may also apply for changes on longer time-scales. Our analysis of ageostrophic processes at Mawson also supports the hypothesis of Parish and Cassano (2003) that orographic blocking is likely to be important as a driver of terrain-constrained flow.

A question that follows is whether locally driven processes are important for ocean circulation in coastal regions. Coupled climate models project a 21st century weakening of zonal mean easterlies under strong forcing scenarios (Neme *et al.*, 2022). Antarctic coastal winds have been linked to ocean circulation across a range of spatial scales (Morrison *et al.*, 2023). For instance, hypothetical changes in the meridional overturning circulation shown by Stewart and Thompson (2012) occur in response to an idealised zonally symmetric wind stress forcing applied over hundreds of kilometres. Other studies emphasise the impacts of wind forcing over the shelf break or in sea-ice producing regions (Morrison *et al.*, 2023; Schmidt *et al.*, 2023; Silvano *et al.*, 2022). Our analysis highlights the central role of large-scale forcing, but there appears to be a close correspondence between regions where additional terms are important (Figure 4b) and regions of Antarctic Bottom Water (AABW) production (Schmidt *et al.*, 2023). Higher spatial resolution is needed to investigate wind dynamics at the spatial scales relevant to AABW production, given that Antarctic coastal polynyas extend at most around 100 km offshore (e.g., based on fig. 1 of Kern (2009)).

One limitation of the approach adopted in this article is that distinguishing large-scale and locally driven processes is not straightforward and our momentum budget assumes a split between the two based on linear extrapolation. As shown by van den Broeke and van Lipzig (2003), however, θ_0 follows the contours of Antarctic orography, meaning the ice sheet has an influence that extends beyond just the temperature deficit layer, and an absence of an Antarctic ice sheet would likely have considerably remote feedbacks on the climate system (e.g., Patterson *et al.*, 2020). Furthermore, Antarctic katabatic drainage flow is thought to feed back on the large-scale pressure gradient, given its spatial scale and potential to transport mass equatorward (Parish & Bromwich, 1997). Model sensitivity experiments are needed to disentangle large-scale forcing entirely from processes originating from the Antarctic ice sheet and sea ice.

5 | SUMMARY AND CONCLUSIONS

The ERA5 reanalysis has been used to characterise the structure and dynamics of coastal easterly winds on sub-daily time-scales and to analyse the momentum

budget dynamics of extremes. In the long-term mean, the balance of acceleration terms offshore is mostly between large-scale forcing, the Coriolis force, and a residual term (mostly friction). In some regions, additional shallow baroclinicity also contributes. Onshore, a more complex balance of terms occurs due to the very large katabatic term and non-negligible horizontal advection.

Across the entire six-hourly period from 2010–2020, 57% of 10-m wind speed variability in the region of the offshore coastal easterlies can be explained by large-scale forcing, increasing to 81% of variability when additional terms associated with the temperature deficit layer and horizontal advection are included. The role of budget terms differs with wind speed, with the residual playing a proportionally larger role at stronger wind speeds. The very strongest winds in ERA5 south of 60°S are notably confined to the Antarctic coastal margins.

Composites of 100 of the most extreme easterly zonal wind events from 2010–2020 show a transient synoptic-scale high–low pressure disturbance concurrent with warm-air advection towards the coast and large-scale and low-level baroclinicity. During the peak of the composite winds, an onshore and offshore low-level jet is present over the coast. After the peak, warmer anomalies persist over the affected region in the lower troposphere and baroclinicity is reduced relative to the pre-peak period. From a detailed analysis of the surface momentum budget offshore and onshore during extreme coastal winds, we find the following.

1. Large-scale forcing is the primary driver behind extreme coastal winds in both offshore and onshore sectors.
2. The shallow baroclinic and katabatic terms play a relatively passive role through the evolution of composited extremes.
3. A southerly anomaly develops in some sectors, which cannot be explained by large-scale forcing, only by the residual term.

The results underscore the distinct dynamics of extreme coastal winds in Antarctica. Although locally driven forcing is important for the six-hourly variability of onshore winds across the entire sampling period, on average its role during the evolution of composited extremes in ERA5 is a passive one. Similarly, extreme offshore coastal easterlies in ERA5 are primarily baroclinic jets, but also with a substantial ageostrophic component in some regions, which we attribute to barrier-jet formation. However, ERA5 underestimates the peak strength of coastal wind extremes. Given the importance of coastal winds for ice sheets, ocean circulation, and sea ice, there is a need to evaluate the representation of these differing dynamical regimes in simulations used for climate projections and for driving ocean models.

DATA AVAILABILITY STATEMENT

Data from the ERA5 reanalysis used in this study are available from the Climate Data Store (https://cds.climate.copernicus.eu/cdsapp#!/home) at https://doi.org/10.24381/cds.143582cf (accessed February 21, 2024). Observational data used in the Supporting Information form part of the SCAR READER dataset available online at https://www.bas.ac.uk/project/reader/ (accessed February 21, 2024).

ORCID

Thomas Caton Harrison https://orcid.org/0000-0001-7870-7039
Thomas J. Bracegirdle https://orcid.org/0000-0002-8868-4739
Hua Lu https://orcid.org/0000-0001-9485-5082

REFERENCES

Armitage, T.W., Kwok, R., Thompson, A.F. & Cunningham, G. (2018) Dynamic topography and sea level anomalies of the southern ocean: variability and teleconnections. *Journal of Geophysical Research: Oceans*, 123, 613–630.

Ball, F. (1960) Winds on the ice slopes of antarctica. In: *Antarctic meteorology*. London: Pergamon, pp. 9–16.

Bintanja, R., Severijns, C., Haarsma, R. & Hazeleger, W. (2014) The future of Antarctica's surface winds simulated by a high-resolution global climate model: 2. Drivers of 21st century changes. *Journal of Geophysical Research: Atmospheres*, 119, 7160–7178.

Blanchard-Wrigglesworth, E., Roach, L.A., Donohoe, A. & Ding, Q. (2021) Impact of winds and southern ocean SSTs on Antarctic sea ice trends and variability. *Journal of Climate*, 34, 949–965.

Bracegirdle, T.J., Connolley, W.M. & Turner, J. (2008) Antarctic climate change over the twenty first century. *Journal of Geophysical Research: Atmospheres*, 113, D03103.

Caton Harrison, T., Biri, S., Bracegirdle, T.J., King, J.C., Kent, E.C., Vignon, É. et al. (2022) Reanalysis representation of low-level winds in the Antarctic near-coastal region. *Weather and Climate Dynamics*, 3, 1415–1437.

Chen, S.-H., McDowell, B., Huang, C.-C. & Nathan, T.R. (2021) Formation of a low-level barrier jet and its modulation by dust radiative forcing over the Hexi Corridor in Central China on

March 17, 2010. *Quarterly Journal of the Royal Meteorological Society*, 147, 1873–1891.

Chen, T.-C., Yau, M.-K. & Kirshbaum, D.J. (2020) Towards the closure of momentum budget analyses in the WRF (v3. 8.1) model. *Geoscientific Model Development*, 13, 1737–1761.

Davrinche, C., Orsi, A., Agosta, C., Amory, C. & Kittel, C. (2023) Understanding the drivers of near-surface winds in Adelie land, East Antarctica. *EGUsphere*, 2023, 1–27.

Dawson, H.R., Morrison, A.K., England, M.H. & Tamsitt, V. (2023) Pathways and timescales of connectivity around the Antarctic continental shelf. *Journal of Geophysical Research: Oceans*, 128, e2022JC018962.

de Brito Neto, F.A., Mendes, D. & Spyrides, M.H.C. (2022) Analysis of extreme wind events in the Weddell Sea region (Antarctica) at Belgrano II station. *Journal of South American Earth Sciences*, 116, 103804.

Descamps, S., Hudson, S., Sulich, J., Wakefield, E., Grémillet, D., Carravieri, A. et al. (2023) Extreme snowstorms lead to large-scale seabird breeding failures in Antarctica. *Current Biology*, 33, R176–R177.

Dong, X., Wang, Y., Hou, S., Ding, M., Yin, B. & Zhang, Y. (2020) Robustness of the recent global atmospheric reanalyses for Antarctic near-surface wind speed climatology. *Journal of Climate*, 33, 4027–4043.

Dutrieux, P., De Rydt, J., Jenkins, A., Holland, P.R., Ha, H.K., Lee, S.H. et al. (2014) Strong sensitivity of pine island ice-shelf melting to climatic variability. *Science*, 343, 174–178.

Ebner, L., Heinemann, G., Haid, V. & Timmermann, R. (2014) Katabatic winds and polynya dynamics at coats land, Antarctica. *Antarctic Science*, 26, 309–326.

Fulton, S.R., Schubert, W.H., Chen, Z. & Ciesielski, P.E. (2017) A dynamical explanation of the topographically bound easterly low-level jet surrounding Antarctica. *Journal of Geophysical Research: Atmospheres*, 122, 12–635.

Gallée, H. & Schayes, G. (1992) Dynamical aspects of katabatic wind evolution in the Antarctic coastal zone. *Boundary-Layer Meteorology*, 59, 141–161.

Gerrish, L., Ireland, L., Fretwell, P. & Cooper, P. (2023) *Medium resolution vector polygons of the Antarctic coastline (7.8)* [Data set]. UK Polar Data Centre, Natural Environment Research Council, UK Research & Innovation. https://doi.org/10.5285/3ea85903-e068-4242-a63f-46767e16f85c

Guest, P., Persson, P.O.G., Wang, S., Jordan, M., Jin, Y., Blomquist, B. et al. (2018) Low-level baroclinic jets over the new arctic ocean. *Journal of Geophysical Research: Oceans*, 123, 4074–4091.

Hazel, J.E. & Stewart, A.L. (2019) Are the near-Antarctic easterly winds weakening in response to enhancement of the southern annular mode? *Journal of Climate*, 32, 1895–1918.

Heinemann, G. & Zentek, R. (2021) A model-based climatology of low-level jets in the Weddell Sea region of the Antarctic. *Atmosphere*, 12, 1635.

Hersbach, H., Bell, B., Berrisford, P., Hirahara, S., Horányi, A., Muñoz-Sabater, J. et al. (2020) The ERA5 global reanalysis. *Quarterly Journal of the Royal Meteorological Society*, 146, 1999–2049.

Kern, S. (2009) Wintertime Antarctic coastal polynya area: 1992–2008. *Geophysical Research Letters*, 36, L14501.

King, J.C., Varley, J.M. & Lachlan-Cope, T.A. (1998) Using satellite thermal infrared imagery to study boundary layer structure in an Antarctic katabatic wind region. *International Journal of Remote Sensing*, 19, 3335–3348.

Labrousse, S., Williams, G., Tamura, T., Bestley, S., Sallée, J.-B., Fraser, A.D. et al. (2018) Coastal polynyas: winter oases for subadult southern elephant seals in East Antarctica. *Scientific Reports*, 8, 1–15.

Lin, X., Zhai, X., Wang, Z. & Munday, D.R. (2020) Southern ocean wind stress in CMIP5 models: role of wind fluctuations. *Journal of Climate*, 33, 1209–1226.

Loescher, K.A., Young, G.S., Colle, B.A. & Winstead, N.S. (2006) Climatology of barrier jets along the Alaskan coast. Part I: spatial and temporal distributions. *Monthly Weather Review*, 134, 437–453.

Mathiot, P., Jourdain, N.C., Barnier, B., Gallée, H., Molines, J.M., Le Sommer, J. et al. (2012) Sensitivity of coastal polynyas and high-salinity shelf water production in the Ross Sea, Antarctica, to the atmospheric forcing. *Ocean Dynamics*, 62, 701–723.

Moore, G. & Renfrew, I. (2005) Tip jets and barrier winds: A QuikSCAT climatology of high wind speed events around Greenland. *Journal of Climate*, 18, 3713–3725.

Morrison, A.K., Huneke, W.G., Neme, J., Spence, P., Hogg, A.M., England, M.H. et al. (2023) Sensitivity of Antarctic shelf waters and abyssal overturning to local winds. *Journal of Climate*, 36, 6465–6479.

Neff, W. (1999) Decadal time scale trends and variability in the tropospheric circulation over the south pole. *Journal of Geophysical Research: Atmospheres*, 104, 27217–27251.

Neme, J., England, M.H. & Hogg, A.M. (2022) Projected changes of surface winds over the Antarctic continental margin. *Geophysical Research Letters*, 49, e2022GL098820.

Olson, J.B., Colle, B.A., Bond, N.A. & Winstead, N. (2007) A comparison of two coastal barrier jet events along the southeast Alaskan coast during the Sarjet field experiment. *Monthly Weather Review*, 135, 2973–2994.

Orr, A., Kirchgaessner, A., King, J., Phillips, T., Gilbert, E., Elvidge, A. et al. (2021) Comparison of kilometre and sub-kilometre scale simulations of a foehn wind event over the Larsen C Ice Shelf, Antarctic Peninsula using the Met Office Unified Model (MetUM). *Quarterly Journal of the Royal Meteorological Society*, 147, 3472–3492.

Overland, J.E. & Bond, N.A. (1995) Observations and scale analysis of coastal wind jets. *Monthly Weather Review*, 123, 2934–2941.

Palarz, A., Luterbacher, J., Ustrnul, Z., Xoplaki, E. & Celiński-Mysław, D. (2020) Representation of low-tropospheric temperature inversions in ECMWF reanalyses over Europe. *Environmental Research Letters*, 15, 074043.

Papritz, L., Pfahl, S., Sodemann, H. & Wernli, H. (2015) A climatology of cold air outbreaks and their impact on air–sea heat fluxes in the high-latitude south pacific. *Journal of Climate*, 28, 342–364.

Parish, T., Pettré, P. & Wendler, G. (1993) The influence of large-scale forcing on the katabatic wind regime at Adélie land, Antarctica. *Meteorology and Atmospheric Physics*, 51, 165–176.

Parish, T.R. (1982) Surface airflow over East Antarctica. *Monthly Weather Review*, 110, 84–90.

Parish, T.R. & Bromwich, D.H. (1987) The surface windfield over the Antarctic ice sheets. *Nature*, 328, 51–54.

Parish, T.R. & Cassano, J.J. (2001) Forcing of the wintertime Antarctic boundary layer winds from the NCEP–NCAR global reanalysis. *Journal of Applied Meteorology*, 40, 810–821.

Parish, T.R. (1983) The influence of the Antarctic Peninsula on the wind field over the western Weddell Sea. *Journal of Geophysical Research: Oceans*, 88, 2684–2692.

Parish, T.R. & Bromwich, D.H. (1997) On the forcing of seasonal changes in surface pressure over Antarctica. *Journal of Geophysical Research: Atmospheres*, 102, 13785–13792.

Parish, T.R. & Bromwich, D.H. (1998) A case study of Antarctic katabatic wind interaction with large-scale forcing. *Monthly Weather Review*, 126, 199–209.

Parish, T.R. & Cassano, J.J. (2003) The role of katabatic winds on the Antarctic surface wind regime. *Monthly Weather Review*, 131, 317–333.

Patterson, M., Woollings, T., Bracegirdle, T.J. & Lewis, N.T. (2020) Wintertime southern hemisphere jet streams shaped by interaction of transient eddies with Antarctic orography. *Journal of Climate*, 33, 10505–10522.

Peña-Molino, B., McCartney, M. & Rintoul, S. (2016) Direct observations of the Antarctic slope current transport at 113°E. *Journal of Geophysical Research: Oceans*, 121, 7390–7407.

Petersen, G.N., Renfrew, I. & Moore, G. (2009) An overview of barrier winds off southeastern Greenland during the Greenland flow distortion experiment. *Quarterly Journal of the Royal Meteorological Society*, 135, 1950–1967.

Pettré, P., Payan, C. & Parish, T.R. (1993) Interaction of katabatic flow with local thermal effects in a coastal region of Adelie land, East Antarctica. *Journal of Geophysical Research: Atmospheres*, 98, 10429–10440.

Renfrew, I.A. (2004) The dynamics of idealized katabatic flow over a moderate slope and ice shelf. *Quarterly Journal of the Royal Meteorological Society*, 130, 1023–1045.

Schmidt, C., Morrison, A.K. & England, M.H. (2023) Wind–and sea-ice–driven interannual variability of Antarctic bottom water formation. *Journal of Geophysical Research: Oceans*, 128, e2023JC019774.

Silvano, A., Holland, P.R., Naughten, K.A., Dragomir, O., Dutrieux, P., Jenkins, A. et al. (2022) Baroclinic ocean response to climate forcing regulates decadal variability of ice-shelf melting in the amundsen sea. *Geophysical Research Letters*, 49, e2022GL100646.

Spence, P., Griffies, S.M., England, M.H., Hogg, A.M., Saenko, O.A. & Jourdain, N.C. (2014) Rapid subsurface warming and circulation changes of Antarctic coastal waters by poleward shifting winds. *Geophysical Research Letters*, 41, 4601–4610.

Stewart, A.L. & Thompson, A.F. (2012) Sensitivity of the ocean's deep overturning circulation to easterly Antarctic winds. *Geophysical Research Letters*, 39, L18604.

Tetzner, D., Thomas, E. & Allen, C. (2019) A validation of ERA5 reanalysis data in the southern Antarctic Peninsula—Ellsworth land region, and its implications for ice core studies. *Geosciences*, 9, 289.

Thompson, A.F., Stewart, A.L., Spence, P. & Heywood, K.J. (2018) The Antarctic slope current in a changing climate. *Reviews of Geophysics*, 56, 741–770.

Tuononen, M., Sinclair, V. & Vihma, T. (2015) A climatology of low-level jets in the mid-latitudes and polar regions of the northern hemisphere. *Atmospheric Science Letters*, 16, 492–499.

Turner, J., Chenoli, S.N., Abu Samah, A., Marshall, G., Phillips, T. & Orr, A. (2009) Strong wind events in the Antarctic. *Journal of Geophysical Research: Atmospheres*, 114, D18103.

Turner, J., Lu, H., King, J., Marshall, G.J., Phillips, T., Bannister, D. et al. (2021) Extreme temperatures in the Antarctic. *Journal of Climate*, 34, 2653–2668.

Turner, J., Phillips, T., Thamban, M., Rahaman, W., Marshall, G.J., Wille, J.D. et al. (2019) The dominant role of extreme precipitation events in Antarctic snowfall variability. *Geophysical Research Letters*, 46, 3502–3511.

Uotila, P., Vihma, T., Pezza, A., Simmonds, I., Keay, K. & Lynch, A. (2011) Relationships between Antarctic cyclones and surface conditions as derived from high-resolution numerical weather prediction data. *Journal of Geophysical Research: Atmospheres*, 116, D07109.

van de Berg, W., Van den Broeke, M. & Van Meijgaard, E. (2007) Heat budget of the East Antarctic lower atmosphere derived from a regional atmospheric climate model. *Journal of Geophysical Research: Atmospheres*, 112, D23101.

van de Berg, W., Van den Broeke, M. & Van Meijgaard, E. (2008) Spatial structures in the heat budget of the antarctic atmospheric boundary layer. *The Cryosphere*, 2, 1–12.

van den Broeke, M. & van Lipzig, N. (2003) Factors controlling the near-surface wind field in Antarctica. *Monthly Weather Review*, 131, 733–743.

van den Broeke, M., Van Lipzig, N. & Van Meijgaard, E. (2002) Momentum budget of the East Antarctic atmospheric boundary layer: results of a regional climate model. *Journal of the Atmospheric Sciences*, 59, 3117–3129.

Vignon, É., Picard, G., Durán-Alarcón, C., Alexander, S.P., Gallée, H. & Berne, A. (2020) Gravity wave excitation during the coastal transition of an extreme katabatic flow in Antarctica. *Journal of the Atmospheric Sciences*, 77, 1295–1312.

Vignon, É., Traullé, O. & Berne, A. (2019) On the fine vertical structure of the low troposphere over the coastal margins of East Antarctica. *Atmospheric Chemistry and Physics*, 19, 4659–4683.

Wang, X., Zhang, Z., Wang, X., Vihma, T., Zhou, M., Yu, L. et al. (2021) Impacts of strong wind events on sea ice and water mass properties in Antarctic coastal polynyas. *Climate Dynamics*, 57, 3505–3528.

Weber, N.J., Lazzara, M.A., Keller, L.M. & Cassano, J.J. (2016) The extreme wind events in the ross island region of Antarctica. *Weather and Forecasting*, 31, 985–1000.

Wei, T., Yan, Q. & Ding, M. (2019) Distribution and temporal trends of temperature extremes over Antarctica. *Environmental Research Letters*, 14, 084040.

Wille, J.D., Favier, V., Gorodetskaya, I.V., Agosta, C., Kittel, C., Beeman, J.C. et al. (2021) Antarctic atmospheric river climatology and precipitation impacts. *Journal of Geophysical Research: Atmospheres*, 126, e2020JD033788.

Wu, Y., Zhai, X. & Wang, Z. (2016) Impact of synoptic atmospheric forcing on the mean ocean circulation. *Journal of Climate*, 29, 5709–5724.

Xu, M., Yang, Q., Clem, K.R., Yu, L. & Hu, X. (2023) On the seasonal and spatial dependence of extreme warm days in Antarctica. *Geophysical Research Letters*, 50, e2022GL102472.

Yu, L. & Zhong, S. (2019a) The interannual variability of surface winds in Antarctica and the surrounding oceans: a climatological analysis using the era-interim reanalysis data. *Journal of Geophysical Research: Atmospheres*, 124, 9046–9061.

Yu, L. & Zhong, S. (2019b) Strong wind speed events over Antarctica and its surrounding oceans. *Journal of Climate*, 32, 3451–3470.

Yu, Y., Cai, X., King, J.C. & Renfrew, I.A. (2005) Numerical simulations of katabatic jumps in coats land, Antarctica. *Boundary-Layer Meteorology*, 114, 413–437.

Zheng, Z., Nie, Y., Chen, X., Jin, J., Chen, Q. & Liu, X. (2022) Historical population dynamics of the Adélie penguin in response to

atmospheric-ocean circulation patterns at Beaufort island, Ross Sea, Antarctica. *Global and Planetary Change*, 216, 103892.

Zhu, J., Xie, A., Qin, X., Wang, Y., Xu, B. & Wang, Y. (2021) An assessment of ERA5 reanalysis for Antarctic near-surface air temperature. *Atmosphere*, 12, 217.

SUPPORTING INFORMATION

Additional supporting information can be found online in the Supporting Information section at the end of this article.

APPENDIX A. SELECTION OF LEVEL *m*

In our implementation of the momentum budget (see Section 2.3), the estimation of the background potential temperature (θ_0) depends on the selection of a model hybrid height level of *m*, which in turn is used to select two levels of constant θ from which θ_0 is linearly extrapolated down to the surface. Here, we show the effect of varying model level *m* on θ_0 and u_{lsc}, the large-scale wind in the cross-slope direction, which in turn is used to obtain lsc$_y$, the most important of the momentum-budget terms identified in this article. A three-day period (August 20–22, 2022) was selected, which has a relatively well-defined temperature deficit layer extending offshore (i.e., a cold pool). A transition from negative cross-slope winds onshore (mostly easterly) to positive cross-slope winds offshore (mostly westerly) is evident, with the largest shear present in the lowest 1000 m (Figure A1a–c), where a layer of more intense winds occurs over the sloping terrain and a disruption to the westerlies occurs within the cold pool offshore. Contours of θ are clustered near the surface, especially in the lowest 1000 m, compared with the more linear profile of θ aloft. Extrapolating the linear θ aloft down to the surface yields the θ_0 shown as dashed grey contours in Figure A1d–f. These match the θ in the Figure A1a–c closely, except near the surface. All three tested *m* values produce qualitatively similar θ_0, though the smoothest is obtained with $m = 100$ (Figure A1e), for which there is little evidence of a near-surface temperature deficit.
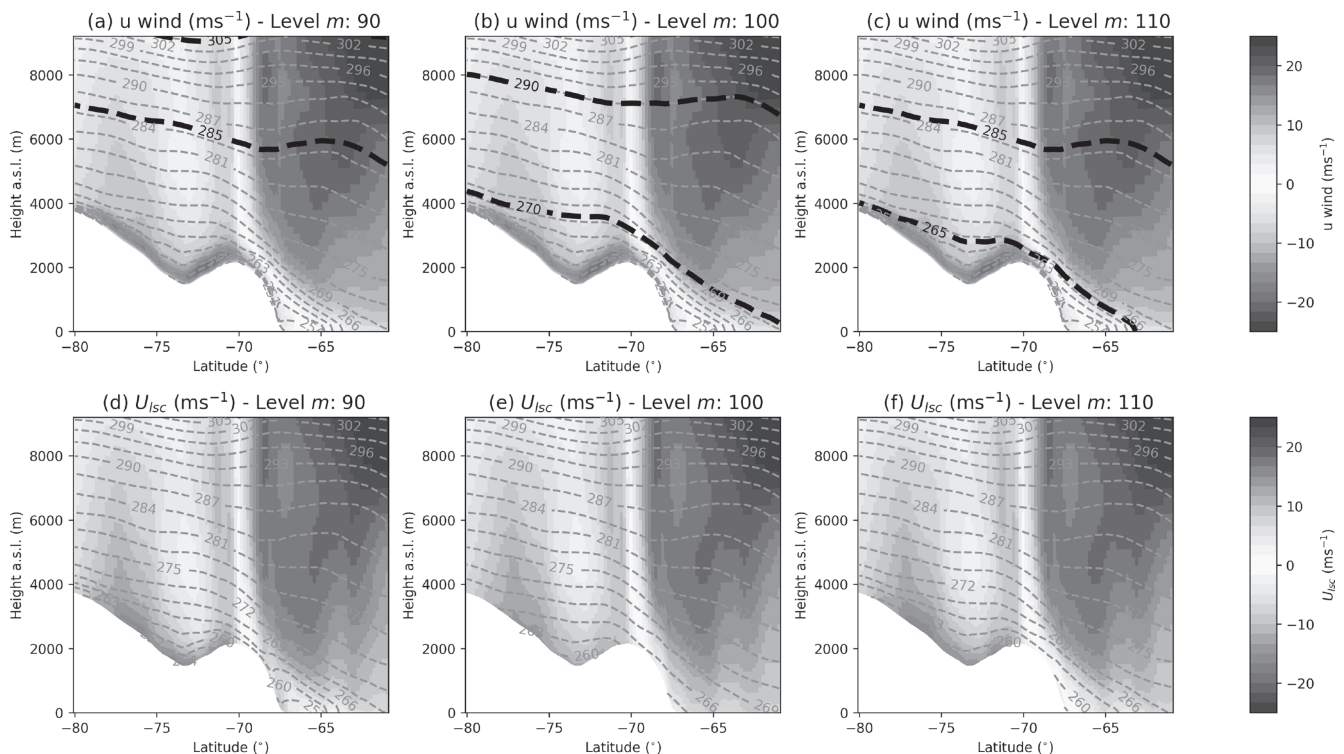

FIGURE A1 Cross-sections through Mawson station (62.87°E) of (a–c) the cross-slope wind *U* (shaded) averaged across August 20–22, 2012. Thick black dashed contours show the two θ levels (the top one obtained from model level *m* and the bottom 20 K lower) used to extrapolate θ_0. Dashed grey contours show θ. (d–f) U_{lsc} for the same period (shaded) calculated using different *m* levels. Dashed grey contours show θ_0. *m* levels tested include (d) 90, (e) 100, and (f) 110. [Colour figure can be viewed at wileyonlinelibrary.com]

As with θ_0 and θ, u_{lsc} (shaded in Figure A1d–f) maps on closely to u (shaded in Figure A1a–c), indicating that for this period the geostrophic wind and thermal wind balance (Equation 5) approximates well to the actual wind. Near the surface, u_{lsc} lacks the strong cross-slope winds seen in u and there is no evidence of the disruption to the westerlies seen in Figure A1a–c, again with the smoothest result occurring for $m = 100$ (Figure A1e). An m of 100 is appropriate, as it selects a sector of the midtroposphere which does not extend above the tropopause (as with $m = 90$) but also does not overlap with the temperature deficit layer (as with $m = 110$). This value of m was tested for a variety of seasons and sectors of Antarctica and found to produce similar results (not shown).